Title

‘Radical interpretations’ preclude the use of climatic wiggle matching for resolution of event timings at the highest levels of attainable precision

Authors

Mark, Darren F
Renne, Paul R
Dymock, Ross C
et al.

Publication Date

2017-10-01

DOI

10.1016/j.quageo.2017.08.003

Peer reviewed

Accepted Manuscript

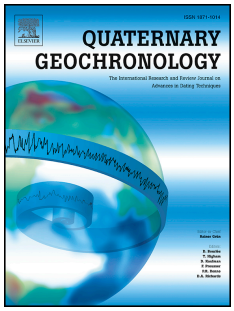

High-precision $^{40}Ar/^{39}Ar$ dating of pleistocene tuffs and temporal anchoring of the Matuyama-Brunhes boundary

Darren F. Mark, Paul R. Renne, Ross Dymock, Victoria C. Smith, Justin I. Simon, Leah E. Morgan, Richard A. Staff, Ben S. Ellis

PII: S1871-1014(17)30005-5

DOI: 10.1016/j.quageo.2017.01.002

Reference: QUAGEO 820

To appear in: *Quaternary Geochronology*

Received Date: 6 February 2016

Revised Date: 10 January 2017

Accepted Date: 15 January 2017

Please cite this article as: Mark, D.F., Renne, P.R., Dymock, R., Smith, V.C., Simon, J.I., Morgan, L.E., Staff, R.A., Ellis, B.S., High-precision $^{40}Ar/^{39}Ar$ dating of pleistocene tuffs and temporal anchoring of the Matuyama-Brunhes boundary, *Quaternary Geochronology* (2017), doi: 10.1016/j.quageo.2017.01.002.

High-precision $^{40}Ar/^{39}Ar$ dating of Pleistocene Tuffs and temporal anchoring of the Matuyama-Brunhes Boundary

Darren F. Mark[1,2]*, Paul R. Renne[3,4], Ross Dymock[1], Victoria C. Smith[5], Justin I. Simon[6], Leah E. Morgan[1,7], Richard A. Staff[5] & Ben S. Ellis[8]

*Corresponding author: darren.mark@glasgow.ac.uk

[1]Scottish Universities Environmental Research Centre, Isotope Geosciences Unit, Rankine Avenue, East Kilbride, Scotland, G75 0QF, UK

[2]Department of Earth & Environmental Science, School of Geography & Geosciences, University of St Andrews, St Andrews, KY16 9AJ, UK

[3]Berkeley Geochronology Center, 2455 Ridge Rd., Berkeley, CA 94709, USA

[4]Department of Earth and Planetary Science, University of California, Berkeley, CA, 94720, USA

[5]Research Laboratory for Archaeology and the History of Art, University of Oxford, Oxford, OX1 3QY, UK

[6]Center for Isotope Cosmochemistry and Geochronology, Astromaterials Research Office KR111, NASA Johnson Space Center, Houston, TX 77058, USA

[7]U.S. Geological Survey, Denver Federal Center, MS 963, Denver, CO 80225, USA

[8]Institute of Geochemistry and Petrology, Department of Earth Sciences, ETH Zurich, Clausiusstrasse 25, 8092 Zürich, Switzerland

Keywords: Matuyama-Brunhes, geomagnetic, $^{40}Ar/^{39}Ar$, Toba, Bishop Tuff, orbital tuning, Australasian Tektite

Abstract

High-precision $^{40}Ar/^{39}Ar$ ages for a series of proximal tuffs from the Toba super-volcano in Indonesia, and the Bishop Tuff and Lava Creek Tuff B in North America have been obtained. Core from Ocean Drilling Project Site 758 in the eastern equatorial Indian Ocean contains discrete tephra layers that we have geochemically correlated to the Young Toba Tuff (73.7 ± 0.3 ka), Middle Toba Tuff (502 ± 0.7 ka) and two eruptions (OTTA and OTTB) related to the Old Toba Tuff (792.4 ± 0.5 and 785.6 ± 0.7 ka, respectively) ($^{40}Ar/^{39}Ar$ data reported as full external precision, 1

sigma). Within ODP 758 Termination IX is coincident with OTTB and hence this age tightly constrains the transition from Marine Isotope Stage 19-20 for the Indian Ocean. The core also preserves the location of the Australasian tektites, and the Matuyama-Brunhes boundary with Bayesian age-depth models used to determine the ages of these events, c. 784 ka and c. 786 ka, respectively. In North America, the Bishop Tuff (766.6 ± 0.4 ka) and Lava Creek Tuff B (627.0 ± 1.5 ka) have quantifiable stratigraphic relationships to the Matuyama-Brunhes boundary. Linear age-depth extrapolation, allowing for uncertainties associated with potential hiatuses in five different terrestrial sections, defines a geomagnetic reversal age of 789 ± 6 ka. Considering our data with respect to the previously published age data for the Matuyama-Brunhes boundary of Sagnotti et al. (2014), we suggest at the level of temporal resolution currently attainable using radioisotopic dating the last reversal of Earths geomagnetic field was isochronous. An overall Matuyama-Brunhes reversal age of 783.4 ± 0.6 ka is calculated, which allowing for inherent uncertainties in the astronomical dating approach, is indistinguishable from the LR04 stack age (780 ± 5 ka) for the geomagnetic boundary. Our high-precision age is 10 ± 2 ka older than the Matuyama-Brunhes boundary age of 773 ± 1 ka, as reported previously by Channell et al. (2010) for Atlantic Ocean records. As ODP 758 features in the LR04 marine stack, the high-precision $^{40}Ar/^{39}Ar$ ages determined here, as well as the Matuyama-Brunhes boundary age, can be used as temporally accurate and precise anchors for the Pleistocene time scale.

Introduction

The Earth's magnetic field alternates between periods of *normal* polarity, in which the mean polarity of the field was the same as the present, and *reverse* polarity, in which the polarity was the opposite. Reversals in geomagnetic field polarity have occurred episodically throughout much of geologic time. To the extent that these polarity

reversals are globally synchronous they can be used as tick marks whose ages, when calibrated, are invaluable components of the Geological Time Scale. Two challenges limit the utility of geomagnetic polarity reversals as time stamps in the geologic record: (1) the unambiguous correlation of magnetic polarity records recovered from rocks or sediments with a global record of such events, and (2) the accuracy of age calibrations. In this paper we address both issues in the case of the reversal between the Matuyama and Brunhes geomagnetic polarity epochs, also known as the Matuyama-Brunhes boundary (MBB), whose age is of fundamental importance to many topics in the Earth Sciences yet has been controversial.

The MBB was the most recent full reversal of the Earth's magnetic field, and serves as a Global Boundary Stratotype Section and Point (GSSP), selected by the International Commission on Stratigraphy as a marker for the beginning of the Middle Pleistocene. An age of 780 ka for the MBB (Shackleton et al., 1990) was determined by orbital tuning of benthic and planktic $\partial^{18}O$ records from Ocean Drilling Program (ODP) Site 677 in the eastern equatorial Pacific (Figure 1). The tuning was calibrated to an ice volume model (Imbrie & Imbrie, 1980), which was based on a series of orbital solutions (Berger & Loutre, 1988). The specific location of the MBB within the ODP 677 core was unknown and hence extrapolation of its location from Deep Sea Drilling Project Site 607 was required (Figure 1). Other orbital tuning ages for the MBB range from 730 ka (Imbrie et al., 1984; Ruddimann et al., 1989) to 790 ka (Johnson, 1982).

An extremely precise orbitally-tuned age of 773 ± 1 ka was recently proposed for the MBB (Channell et al., 2010). Five North Atlantic records placed in isotope age models that were constructed by correlation of the $\partial^{18}O$ record directly or indirectly to an ice volume model were used to place the MBB consistently at the young end of Marine Isotope Stage (MIS) 19. The orbitally-tuned MBB age inferred by Channell et al. (2010) was stated to be consistent with an $^{40}Ar/^{39}Ar$ age (776 ± 2 ka, 1 sigma, analytical uncertainty only), (Coe et al., 20041) from Hawaiian lavas, but only if the

age of Fish Canyon sanidine (FCs), a secondary mineral standard for the $^{40}Ar/^{39}Ar$ radio-isotopic dating system, is adjusted to an age of 27.93 Ma – an age known from numerous studies to be too young (e.g., Kuiper et al., 2008; Renne et al., 2011; Rivera et al., 2011; Wotzlaw et al., 2013; Morgan et al., 2014). Remarkably, Singer (2014) subsequently reanalysed the same Hawaiian lavas and obtained the identical result of 776 ± 1 ka (1 sigma, analytical uncertainty only) but using a different $^{40}Ar/^{39}Ar$ calibration (decay constants of Min et al., 2000 and the FCs age of 28.201 Ma, Kuiper et al., 2008). The perfect congruence of these two ages is spurious, however, as applying the same calibration to both $^{40}Ar/^{39}Ar$ ages (Coe et al., 2004; Singer, 2014) indicates that they differ by 5 ± 3 ka.

Direct radio-isotopic ages have been determined for the MBB through $^{40}Ar/^{39}Ar$ dating of various lava flows with transitional directions or known relationships to the MBB. Baksi et al. (1992) dated lavas from Maui with transitional paleomagnetic directions related to the MBB to yield an $^{40}Ar/^{39}Ar$ age of 783 ± 11 ka (1 sigma, analytical uncertainty only) using the decay constants of Steiger & Jager (1977) and the SB3 biotite standard at 162.9 Ma, which is equivalent to Fish Canyon sanidine (FCs) at 27.5 Ma (Lanphere & Baadsgaard, 2001). Recalculated[^] this age is 795 ± 11/12 ka. Singer and Pringle (1996) determined an $^{40}Ar/^{39}Ar$ weighted mean age for 8 basaltic to andesitic lava flows inferred to have erupted during the MB-reversal from Chile, Tahiti, La Palma and Maui. They calculated an age (779 ± 2 ka, 1 sigma, analytical) using the decay constants of Steiger & Jager (1977) and the Taylor Creek sanidine (TCs) standard with an age of 27.9 Ma, which is also equivalent to FCs at 27.5 Ma. Recalculated the MBB age of Singer and Pringle (1996) is 791 ± 2/3 ka. Singer et al. (2005) incorporating the data of Coe et al. (2004) proposed that there were two age clusters for MBB-related lava flows: (1) 776 ± 2 ka

[^] Unless otherwise stated all $^{40}Ar/^{39}Ar$ ages are re-calculated using the optimisation model of Renne et al. (2010), the decay constants of (Renne et al., 2011) and an Alder Creek sanidine (ACs) age of 1.1891 Ma (Niespolo et al., 2016). All data are reported as X ± Y/Z, where Y is analytical uncertainties and Z is full external precision, including uncertainties from the decay constant. The confidence interval is 68.2 % confidence (1 sigma).

(1 sigma, analytical uncertainty), and (2) 793 ± 3 ka (1 sigma, analytical uncertainty). These ages were calculated using the decay constants of Steiger & Jager (1977) and TCs with an age of 28.34 Ma, which is equivalent to an FCs age of 28.02 Ma (Renne et al., 1998). Recalculated these ages are 773 ± 2/3 ka and 790 ± 3/3 ka, respectively. It was proposed that the older age was related to an initial demise of the axial dipole, onset of geodynamo instability, and non-dipolar field behaviour – a precursor to reversal of field polarity. A MBB precursor event with low field intensity has been noted in some (Kent & Schneider, 1995; Hartl & Tauxe, 1996; Channell et al., 2009, 2010) but not all marine records (e.g., Suganuma et al., 2014). Importantly, there is no direct palaeomagnetic evidence linking the older age of Singer et al. (2005) to such a precursor event. As discussed (above), Singer (2014) made new measurements on old MBB-related samples (Coe et al., 2004), giving a recalculated age of 779 ± 1/1 ka.

The dating of silicic tuffs that straddle the MBB has vast potential for determination of accurate and precise event timings with robust, fully quantifiable uncertainties, especially if high-K phases such as sanidine/anorthoclase are present for $^{40}Ar/^{39}Ar$ analyses. The sanidine- and zircon-bearing Bishop Tuff (BT) deposited below the Lava Creek Tuff Member B (LCTB) but above the MBB, has been the focus of much interest. Briefly, Sarna-Wojcicki et al. (2000) calculated sedimentation rates in terrestrial sections throughout western North America making the simple (but geologically tenuous) assumption of constant sedimentation rate between the LCTB and the BT. Employing the inferred sedimentation rates, they calculated the duration between the BT and the MBB represented by the intervening sediment. These results, that are independent of which calibration of the $^{40}Ar/^{39}Ar$ system is used, imply that the MBB is 15 ± 2 ka older than the BT assuming the validity of the assumed uniform sedimentation rates. Unfortunately, the age of the Bishop Tuff has remained controversial and hence its reliability for determination of an age for the MBB has been questioned (e.g., Channell et al., 2010).

The age, character and tempo of the MBB was clarified by recent high-precision $^{40}Ar/^{39}Ar$ dating of sanidine from tephra layers that bracket the boundary within the Sulmona Basin paleolake in Central Italy (Sagnotti et al., 2014; Giaccio et al., 2015). The lacustrine sediments within which the tuffs are intercalated are characterized by biogenic magnetite and were sampled at high resolution, allowing the reconstruction of the MBB in very fine detail. The Sulmona results show that the MBB is significantly older than 773 ± 1 ka (Channell et al., 2010) with a recalculated age of 783 ± 1/1 ka. Using the same parameters but the weighted mean astronomical ACs age rather than the Optimisation Model ACs age (Niespolo et al., 2016), the Sulmona data yield a MBB age of 780 ± 1/1 ka (Sagnotti et al., 2014), both ages resolvably older (10 ± 2 ka and 7 ± 2 ka, respectively) than 773 ± 1 ka.

Most recently U-Pb SHRIMP-II ages have been determined for a tephra associated with the MBB in Japan (Suganuma et al., 2014). However, primarily for reasons highlighted by Ickert et al. (2015) and discussed by us in detail below, we do not consider either the U/Pb data accurate or appropriate for use in determining an age for the MBB (i.e., poor characterisation of Th/U_{melt} from which the zircons grew). Further, Suganuma et al. (2014) failed to disequilibrium-correct their Tera-Wasserburg relations, the oxygen isotope data are of inadequately low resolution to precisely define the boundaries of MIS 19, and there are no quantitative constraints for the sedimentation rate.

The MB-reversal: isochronous or diachronous?

Owing to large degrees of scatter in the data that attempt to temporally anchor the MBB there has been the suggestion that the reversal was diachronous on a global-scale (e.g., Rivera et al., 2011). Until recently the MB-reversal, as with other geomagnetic polarity reversals, has been considered isochronous, certainly at the relatively poor levels of temporal resolution (accuracy and precision) attained using

the $^{40}Ar/^{39}Ar$ geochronometer between 1990 and 2010. However, computer modeling of the MB-reversal has highlighted potential for a millennial-scale (± 1 ka) offset in the onset of the polarity reversal for sites in the Atlantic and Pacific Oceans (Leonhardt & Fabian, 2007). The study also proposed reversal durations of between 2-10 ka, which exceeds the MBB duration recorded by the high-resolution record at Sulmona by more than an order of magnitude (Sagnotti et al., 2016).

Ocean Drilling Project (ODP) Leg 758

Ocean Drilling Project (ODP) Site 758 resides on the crest of Ninetyeast Ridge (5˚23.05'N, 90˚21.67'E) in a water depth of 2,924 m (Figure 1). Three holes were cored at Site 758 (A, B, C). Within the timeframe of interest (Holocene-Pleistocene) stratigraphic analysis showed good recovery (Shipboard Scientific Party, 1989). Due to the possibility of gaps occurring between successive Advanced Piston Corer (APC) core sections, sections in ODP 758A and ODP 758B were staggered in depth relative to each other. It was possible to provide high-resolution between-hole correlation by using a combination of paleomagnetic remanence, magnetic susceptibility and distinct lithological and tephra markers (Shipboard Scientific Party, 1989; Dehn et al., 1991; Farrell & Janecek, 1991; Gee et al., 1991).

There were two defined scientific aims for drilling Site 758: (1) to study the tephrochronology of the Indonesian volcanic arc relative to a changing climate signal, and (2) to study in detail the behaviour of Earth's magnetic field during polarity transitions. As such the ODP 758 deep sea core contains: (1) records of distal tephras (volcanic ash layers) from the Indonesian volcanic arc above and below the MBB (Dehn et al., 1991), (2) cm-scale resolution $\partial^{18}O$ records from benthic and planktic foraminifera (Farrell & Janecek, 1991; Chen et al., 1995), and (3) a detailed paleomagnetic stratigraphy that shows the precise and well-defined location of the

MBB, as well as the onset and termination of the Jaramillo Geomagnetic Excursion (JGE) (Shipboard Scientific Party, 1989; Gee et al., 1991).

ODP 758 Tephrochronology

The tephra layers documented within Site 758 provide a unique record of explosive volcanism for the North Indian Ocean. Over 200 visible tephra (ash) layers have been documented from the site ranging in thickness from millimetres to decimetres. Many of the tephras are present in one hole but not in the neighbouring holes. The tephras also display variable forms, ranging from discrete to diffuse layers and patches/pods of ash. The local absence and variable physical characteristics of a given tephra is due to the variety of depositional processes operating on the crest of the Ninetyeast Ridge (Dehn et al., 1991) and hence not unexpected (Carey, 1997). Given the distance (Figure 1) between Site 758 and the Indonesian volcanic arc (the most proximal and therefore probable volcanic source) the tephra found in the three holes are distal in nature, fine-grained and dominated by glass shards rather than mineral grains. As such the tephras are unsuitable for direct $^{40}Ar/^{39}Ar$ dating due to paucity of required mineral phases.

Two of the distal tephras located in ODP 758 have been robustly correlated using glass and mineral chemistry to the Young Toba Tuff (YTT, Ash A, *c.* 74 ka; Mark et al., 2014, Storey et al., 2012) and Middle Toba Tuff (MTT, Ash C, *c.* 500 ka; Chesner et al., 1991) eruptions of the Toba super-volcano (Dehn et al., 1991) (Figure 1). Older ash units (E, *d* and D) have been the focus of much attention with the question raised as to which, if any, correlates with the oldest super-eruption (Old Toba Tuff, OTT, *c.* 800 ka; Chesner et al., 1991) of Toba (Shane et al., 1995). Lee et al. (2004) linked Ash D with OTT but this correlation was subsequently questioned (Chen et al., 2004; Shane et al., 2004). Further geochemical work is required to confidently link these ashes to proximal deposits, and to determine whether or not

their source was indeed Toba. Note, the age of Ash D was calibrated by astronomically tuned oxygen isotope stratigraphy to 788.0 ± 2.2 ka (Lee et al., 2004).

Paleomagnetic data of ODP 758.

In addition to containing discrete tephra layers, ODP 758 contains records of geomagnetic reversals and excursions – the relationships between the tephra and geomagnetic are quantifiable. For the purpose of this discussion/study we have focussed on the composite ODP 758 record (ODP 758A, 758B, 758C) as presented by Farrell & Janecek (1991) (Figure 2). By constructing a composite depth section from Holes 758A and 758B it was possible to splice across recovery gaps with the result being an undisturbed, continuous sedimentary section that extends from 0 to 116 mbsf, which is equivalent to the past *c.* 7 Ma (well beyond the time interval of interest for this study). The continuity of this composite section was checked with several independent stratigraphies (e.g., Farrell & Janecek, 1991). The paleomagnetic data for ODP 758 are not ideal in that it was not collected from discrete samples; the U-channel and on-board measurements have in all probability smoothed the paleomagnetic signal, but the core still retains clear transition zones and paleomagnetic directional changes (Shipboard Scientific Party, 1989; Dehn et al., 1991; Farrell & Janecek, 1991; Gee et al., 1991).

The location of the MBB at Site 758

Chen et al. (1995) determined an astronomical age of *c.* 784 ka for the MBB in ODP 758. Although similar to the MBB age of Shackleton et al. (1990) (780 ka) there is no uncertainty associated with these ages and as such, it is unclear whether the offset is 'real' (i.e., geological or methodological). However, it has been suggested that any astronomically tuned age for this period of time cannot be defined

253 better than to within ± 5 ka due to uncertainties in the phase relationship between
254 insolation and climate (Martinson et al., 1987; Imbrie & Imbrie, 1980). The tuning
255 approach of Chen et al. (1995) did vary from that of Shackleton et al. (1990),
256 whereas the latter tuned their $\partial^{18}O$ data to the model of Imbrie & Imbrie (1980) from 0
257 to 1.6 Ma, and to the obliquity cycles from 1.6 to 2.6 Ma, Chen et al. (1995) tuned
258 their entire record to the ice volume simulation based on the model of Imbrie & Imbrie
259 (1980). This approach allowed for a fine tuning approach of both the 41 and 23 ka
260 cycles simultaneously.

261 The ODP 758 $\partial^{18}O$ data (also a composite of $\partial^{18}O$ measurements from ODP
262 758A and ODP 758B; Farrell & Janecek, 1991; Chen et al., 1995) show the location
263 of the MBB in the early part of Marine Isotope Stage (MIS) 19 (Figure 2), earlier than
264 the position of the MBB as noted by Channell et al. (2010) in the North Atlantic. This
265 is not uncommon; the MBB has been identified in the middle of MIS 19 (Suganuma
266 et al., 2014), at the start of MIS 19 (Horng et al., 2002) and even within MIS 20
267 (Langereis et al., 1997), although the latter was attributed to delayed acquisition of
268 the Earth's magnetic signal in the sediment (i.e., lock-in of paleomagnetic
269 remanence) (Kent, 1973). As a consequence, two important questions emerge: (1)
270 should we expect the MBB to be globally located at the exact same location within a
271 MIS? And (2) if so, why do we see such variation in the location of the MBB in
272 different $\partial^{18}O$ records? We consider these to be questions of temporal and spatial
273 resolution within records - we revisit this discussion below.

274

275 The Jaramillo Geomagnetic Excursion at Site 758

276

277 The Jaramillo geomagnetic excursion (JGE) was a reversal of the geomagnetic field
278 that occurred *c.* 1,000 ka (Singer, 2014; Kissel et al., 2014) and is also preserved
279 within ODP 758. It was a short-term reversal in the Matuyama reversed magnetic
280 chronozone. Within ODP 758 the JGE_{onset} is dated at *c.* 1070 ka and the $JGE_{termination}$

281 at *c.* 997 ka (Chen et al., 1995). The Toba tephra are positioned above the JGE
282 within ODP 758.
283
284 Australasian microtektites
285
286 Australasian microtektites have been found below the MBB within sediment cores
287 from throughout the Indian Ocean, western equatorial Pacific Ocean, Philippine, Sulu
288 and Celebes Seas, and most recently the South China Sea (Hyodo et al., 2011 and
289 references within). The Australasian tektites have previously been dated by $^{40}Ar/^{39}Ar$
290 at 799.2 ± 3.4/3.8 ka (Smit et al., 1991) with the data of Yamei et al. (2000)
291 reproducing this age but suggesting the presence of excess ^{40}Ar (noted from
292 isochron analysis of the data, Yamei et al., 2000). As such, the current $^{40}Ar/^{39}Ar$ age
293 for the Australasian microtektites should be considered as a maximum age
294 constraint.
295 Within Site 758 the peak abundance of Australasian microtektites occurs 8
296 cm below a tephra horizon labelled as Ash 'D' and immediately prior to Termination
297 IX (Lee et al., 2004). We know from other Pacific and Indian Ocean records that the
298 Australasian Tektite peak concentration is located immediately prior to Termination
299 IX (e.g., Glass & Koeberl, 2006; Valet et al., 2014), the transition from Marine Isotope
300 Stage (MIS) 19 to 20. Despite a large degree of dispersion throughout the core, the
301 Australasian Tektites main concentration peak is in the correct stratigraphic position
302 relative to other cores from throughout the region.
303
304 ODP 758 and LR04
305
306 LR04 is a 5,300 ka stack of $\partial^{18}O$ records from 57 globally distributed sites that have
307 been aligned using an automated graphic correlation algorithm (Lisiecki & Raymo,
308 2005). This was the first Pliocene-Pleistocene stack to contain more than three

309 records that extend back beyond 850 ka. The LR04 stack contains the composite
310 ODP 758 core data. As an automated graphic correlation algorithm was used to
311 construct the stack, its stratigraphic features are therefore independent of any time
312 scale. An age model was subsequently constructed by aligning the benthic $\partial^{18}O$
313 stack to a simple model of ice volume whilst taking into consideration the average
314 stacked sedimentation rate of the individual sediment cores. The LR04 stack places
315 the MBB at *c.* 780 ka (following Shackleton et al., 1990).
316
317 **Study scope**
318
319 Using a combination of tephrochronology and high-precision $^{40}Ar/^{39}Ar$ geochronology
320 we aim to examine the temporal relationship between the Toba tephra layers
321 preserved in ODP 758 to primarily constrain the age of the MBB, the Australasian
322 Tektites and Termination IX within the Indian Ocean. Furthermore, we examine the
323 relationship of the MBB to the Bishop Tuff and Lava Creek Tuff B (LCTB) in North
324 America. Our findings agree perfectly with those of Sagnotti et al. (2014) and further
325 question the accuracy of the Channell et al. (2010) MBB age estimation, unless an
326 'extremely' diachronous reversal is invoked, an event that our data discount.
327
328 **Field Relations, proximal tuffs: Sumatra**
329
330 Fieldwork was conducted on Sumatra to directly sample the relevant proximal
331 (crystal-rich) Toba deposits. Sampling locations at Siguragura and Haranggoal are
332 shown in Figure 3 with the respective stratigraphies. Owing to the proximal location
333 of the sampling sites to the caldera and abundant rainforest vegetation, correlation of
334 deposits across the caldera is extremely difficult but has been attempted previously
335 by Knight et al. (1986) and Chesner et al. (1991).
336

Haranggoal (N 2˚53,233' E 98˚39.850')

Numerous Toba units are intermittently exposed along the road that climbs the caldera wall near Haranggoal. Andesitic lavas, dated at *c*. 1.3 Ma (Chesner et al., 1991), are exposed at the present lake level. The *c*. 1.2 Ma Haranggoal dacite tuff (HDT) overlies the andesitic lava flows (Chesner et al., 1991). The HDT is a brown, densely welded and often-jointed (radial and columnar) ignimbrite with large, lightly coloured, flattened pumices that reach 1 m in length. Stratigraphically above the HDT are three further units. Chesner et al. (1991) $^{40}Ar/^{39}Ar$ dated the middle 1 m-thick unit at this locality to *c*. 501 ka and noted that it had a normal paleomagnetic polarity. The unit was ascribed to the MTT. Although there is a unit residing between the HDT and the MTT, Knight et al. (1986) and Chesner et al. (1991) assumed the OTT to be absent from this section and that the unit underlying the dated MTT horizon to be another MTT eruption product with slightly different appearance. The unit underlying the MTT is not characteristic of the other OTT deposits reported from elsewhere around the lake; the unit is a dark glassy vitrophyre that is often columnar jointed, and the unit grades to light grey welded ignimbrite with dark fiamme. We now know that the underlying unit is not the MTT but an older eruption product (discussed below). The YTT unit caps the sequence at Haranggoal.

Siguragura (N 2˚31.283' E 99˚16.483')

Chesner and Rose (1991) described the Old Toba Tuff at Siguragura. They, like us, found the OTT to be well exposed on the Uluan block, SE of the lake, where it is a very thick (>300 m in most locations) densely welded ignimbrite that is brown to light grey in colour with abundant fiamme (up to 30 cm). The OTT is often columnar jointed and numerous flow units are observed at some locations. The OTT sample

from Siguragura was $^{40}Ar/^{39}Ar$ dated by Diehl (1987) (*c.* 840 ka) and noted to have a reversed paleomagnetic polarity.

Field Relations, proximal tuffs: North America

Bishop Tuff

The Bishop Tuff has been described in detail by many other studies (e.g., Simon et al., 2014; Ickert et al., 2015) and hence here we just provide details of specific sampling sites. Three samples of the Bishop Tuff, each representing distinct phases of the eruption, were sampled. Localities and ignimbrite subpackage designations (WH1997) refer to Wilson and Hildreth (1997). JIS09MLV33 (BR1): Near-vent facies in the Mono lobe. A single large pumice clast ~8,000 cm^3 was collected from locality 208 in subpackage Ig2NWa (WH1997), at N 37°45.814' latitude, W 118°59.836' longitude. BR11-3: Fall deposit approximately 42 km from the vent in the Tableland lobe. Multiple pumice clasts from ~10-700 cm^3 were collected from locality 16/17 in subpackage Ig2E (WH1997), at N 37°27.578' latitude, W 118°21.990' longitude. BR11-4: Near-vent facies in the Gorges lobe. A single block of densely welded tuff ~3,000 cm^3 was collected from near locality 444 in subpackage Ig1Eb (WH1997), at N 37°35.288' latitude, W 118°42.284' longitude.

Lava Creek Tuff B

Similarly, the Lava Creek Tuff B (LCTB) has been described in detail by many other studies (e.g., Wotzlaw et al., 2015) and as such, details of just the sampling site are described. The LCTB ignimbrite was sampled from the location described by Christiansen (2001) at the quarry near the east end of the dam at Grassy Lake Reservoir, just south of Yellowstone National Park (N44°13.074', W110°81.417').

The sample was from the relatively crystal-rich densely welded basal vitrophyre of the ignimbrite. Bulk composition of this sample is identical to compositions of LCTB reported by Christiansen (2001).

Analytical methods

Electron microprobe glass and biotite geochemistry

Major element compositions of glass and biotite from both the proximal Toba deposits (YTT, MTT, OTT) and distal deposits (Ash layers A, C, d, D, E) were determined using a wavelength-dispersive JEOL 8600 electron microprobe (EMP) at the Research Laboratory for Archaeology and the History of Art, University of Oxford. The instrument was calibrated at 15 kV using a range of mineral standards. A low beam current (6 nA), and defocused (10 μm) beam were used to analyse individual glass shards. Single biotite crystals were analysed with a beam current of 15 nA, and a 5 μm beam. Peak counting times were 30 s for all elements except Na (10 s in glass and 20 s in biotite). The EMP calibration was verified using a range of reference glasses from the Max Planck Institut (Jochum et al., 2006) and minerals from the Smithsonian (Jarosewich et al., 1980). Totals of glass analyses were mostly >95% and normalized to 100% to account for variable secondary hydration. Biotite analytical totals were typically >92 wt.%. All raw analyses of the glass and biotite, and the reference materials are included in appendix file 'SF#1' (.pdf).

$^{40}Ar/^{39}Ar$ dating

A detailed sample preparation routine is discussed by Mark et al. (2010) but briefly: feldspars (sanidine) were separated from approximately 2 kg of each sample after disaggregating, washing and sieving followed by magnetic and density separations

and finally ultrasonic cleaning in 5% hydrofluoric acid for 5 minutes. Feldspars were handpicked under binocular microscope for analysis. Samples were irradiated in the CLICIT facility of the Oregon State University TRIGA reactor using the Alder Creek sanidine (Nomade et al., 2005) as a neutron fluence monitor.

$^{40}Ar/^{39}Ar$ analyses were conducted at the NERC Argon Isotope Facility, Scottish Universities Environmental Research Centre (SUERC) and the Berkeley Geochronology Center (BGC). Samples analyzed at BGC were run and reported blindly, without knowledge of the SUERC results (and vice versa). Details of irradiation durations, J measurements, discrimination corrections are provided in appendix file SF#3b (.pdf). Irradiation correction parameters are shown below.

For J determinations three bracketing standard positions surrounding each unknown were used to monitor the neutron fluence. Ten measurements were made for each bracketing standard position. The weighted average $^{40}Ar^*/^{39}Ar_K$ was calculated for each well, and the arithmetic mean and standard deviation of these three values was used to characterize the neutron fluence for the unknowns. This approach was deemed sufficient as, due to the relatively short irradiation durations, there was no significant variation between the three positions in a single level of the irradiation holder. This also facilitated high-precision measurement of the J-parameter. Note that for all J-measurements no data were rejected.

Samples were analyzed in several batches; backgrounds and mass discrimination measurements (via automated analysis of multiple air pipettes) specific to each batch are summarized in appendix file 'SF#1' (.pdf). Air pipettes were run (on average) after every 5 analyses. Backgrounds subtracted from ion beam measurements were arithmetic averages and standard deviations. Mass discrimination was computed based on a power law relationship (Renne et al., 2009) using the isotopic composition of atmospheric Ar reported (Lee et al., 2006) that has been independently confirmed (Mark et al., 2011). Corrections for radioactive decay of ^{39}Ar and ^{37}Ar were made using the decay constants reported by Stoener et al.

(1965) and Renne & Norman (2001), respectively. Ingrowth of ^{36}Ar from decay of ^{36}Cl was corrected using the $^{36}Cl/^{38}Cl$ production ratio and methods of Renne et al. (2008) and was determined to be negligible. Argon isotope data corrected for backgrounds, mass discrimination, and radioactive decay and ingrowth are given in the appendix file 'SF#1' (.pdf).

At SUERC the samples were analyzed by total fusion and step-heating with a CO_2 laser and measurements made using a MAP 215-50 (MAP2) noble gas mass spectrometer. The mass spectrometer is equipped with a Nier-type ion source and analogue electron multiplier detector. Mass spectrometry utilized peak-hopping by magnetic field switching on a single detector in 10 cycles.

At BGC the samples were analyzed by total fusion with CO_2 lasers on two different extraction systems mated to MAP 215 mass spectrometers (MAP1 and MAP3). MAP1 is a 215C and MAP3 is a 215-50. Both have Nier-type ion sources and analog electron multiplier detectors. Mass spectrometry utilized peak-hopping by magnetic field switching on a single detector in 10-15 cycles.

Ages were computed from the blank-, discrimination- and decay-corrected Ar isotope data after correction for interfering isotopes based on the following production ratios, determined from fluorite and Fe-doped $KAlSiO_4$ glass: $(^{36}Ar/^{37}Ar)_{Ca}$ = (2.650 ± 0.022) x 10^{-4}; $(^{38}Ar/^{37}Ar)_{Ca}$ = (1.96 ± 0.08) x 10^{-5}; $(^{39}Ar/^{37}Ar)_{Ca}$ = (6.95 ± 0.09) x 10^{-4}; $(^{40}Ar/^{39}Ar)_{K}$ = (7.3 ± 0.9) x 10^{-4}; $(^{38}Ar/^{39}Ar)_{K}$ = (1.215 ± 0.003) x 10^{-2}; $(^{37}Ar/^{39}Ar)_{K}$ = (2.24 ± 0.16) x 10^{-4}, as determined previously for this reactor in the same irradiation conditions (Renne et al., 2004). Ages and their uncertainties are based on the methods of Renne et al. (2010), the calibration of the decay constant as reported by Renne et al. (2011) and the ACs optimization age (1.1891 ± 0.0009 Ma, R_{FCs}^{ACs}: 0.041707 ± 0.000011, 1 sigma) as reported by Niespolo et al. (2016), except where noted. The optimization-modeled age for the ACs standard has accurate quantifiable uncertainties and hence is favored here over the astronomically tuned

ACs age presented by Niespolo et al. (2016). The reason for this is that the astronomical calibration has unknown uncertainty and confidence intervals and uses best guess 'assumptions' to constrain, for example, phase relationships between insolation and climate within the Pleistocene.

For some of the age comparisons made herein, contributions from sources of systematic uncertainty (i.e., uncertainties in $^{40}Ar/^{40}K$ of the standard and ^{40}K decay constants) are neglected and only analytical uncertainties in isotope measurements of samples and standards are included. These uncertainties are referred to herein as "analytical precision". For the purposes of this study analytical uncertainties include contributions from uncertainties in the interference corrections because these interference corrections have variable effects due to the slight variable chemistry of the samples considered. Where not otherwise distinguished, uncertainties are stated as X ± Y/Z, where Y is the analytical uncertainty as defined above, and Z is the full external precision considering both analytical and systematic sources of uncertainty (e.g., decay constant).

Age computation uses the weighted (by inverse variance) mean of $^{40}Ar^*/^{39}Ar_K$ values for the sample and standard, combined as *R*-values and computed using the method of Renne et al. (2010). Outliers in both single-crystal samples and standards were discriminated using a 3-sigma filter applied iteratively until all samples counted are within 3 standard deviations of the weighted mean ± one standard error. This procedure screened older crystals that are logically interpreted as xenocrysts. No younger outliers were recorded during analysis of all samples. Processing of the data using the *n*MAD approach of Kuiper et al. (2008) has no impact on the probability distribution plots for each sample.

The analytical approach adopted was to initially analyze at all times single crystals of sanidine by total fusion (SUERC & BGC). Following the initial analyses if no xenocrystic contamination was observed, samples of small crystal populations (*n*3) were step-heated (SUERC). The purpose of the step heating was to verify that

503 initial trapped $^{40}Ar/^{36}Ar$ compositions overlap with accepted atmospheric values (Lee
504 et al., 2006; Mark et al., 2011).
505
506 **Results**
507
508 Fieldwork & tephra geochemistry
509
510 There are limited accessible outcrops around Lake Toba that preserve a full volcanic
511 stratigraphy. Hence the eruption history of Toba has been pieced together from distal
512 locations (e.g., marine cores) and a couple of non-correlated sites located proximal
513 to the caldera. As discussed above, we sampled the deposits at two of these key
514 localities, Haranggoal at Siguragura (Figure 3), as the volcanic units preserved at
515 these localities have been previously ascribed to the three different Toba eruptions
516 (OTT, MTT and YTT). At Siguragura the OTT unit is unconformably overlain by the
517 YTT. The YTT is also preserved at Harrangoal and is underlain by two units ascribed
518 to the MTT, which lie above the Harrangoal Dacitic Tuff (HDT, Shane et al., 1995;
519 Lee et al., 2004). Although the lowermost unit lies within the same stratigraphic
520 position as OTT, it was assumed to be the MTT, as it appears texturally different in
521 appearance from the OTT at Siguragura.
522 Interestingly, within ODP 758 there are two tephras of the approximate age of
523 the OTT, Ash d and Ash D. We hypothesized that the OTT deposits at Siguragurra
524 and Harrangoal are products of two different eruptive events that occurred *c.* 800 ka,
525 which correspond to Ash D (*termed* OTTB, Haranggoal) and Ash *d* (*termed* OTTA,
526 Siguragura) in the distal ODP 758 core. Our geochemical data on both glass and
527 biotite (Figure 4) show that despite a different appearance, this lower presumed MTT
528 unit at Haranggoal is compositionally indistinguishable from the other OTT proximal
529 deposits and that indeed Ash d and Ash D correspond to two different eruptions that
530 occurred about the same time as 'the OTT' (hence labelling OTTA and OTTB).

Based upon the previously published estimated sedimentation rate in ODP 758 of 1.7 cm/ka (Farrell & Janecek, 1991), there would be *c.* 6 ka between Ash *d* and Ash D.

$^{40}Ar/^{39}Ar$ dating results

All of our new $^{40}Ar/^{39}Ar$ data are presented in Figures 5-8. Pooled ages for the two samples dated by both SUERC and BGC are calculated from the weighted mean *R*-values (Renne et al., 1998) corresponding to the single crystal total fusion measurements for each sample. All data are presented at the 1 sigma confidence level and are summarized in Table 1.

OTTA$_{total\ fusion\ (pooled)}$*:* SUERC analysed 61 crystals and BGC analysed 40 crystals (sample NP1). One data point was rejected due to the analysis of a plagioclase grain rather than a sanidine crystal. Data define a weighted mean pooled age of 792.5 ± 0.5/0.6 ka (Figure 5).

OTTA$_{step\text{-}heating}$: SUERC performed four step-heating experiments on four different aliquots of sanidine crystal populations (*n*3) (sample NP1). All experiments yielded 100% ^{39}Ar plateaux with initial $^{40}Ar/^{36}Ar$ trapped components that overlapped with atmospheric values (Lee et al., 2006). The weighted mean plateau age (791.9 ± 1.0/1.1 ka) and inverse isochron age (Figure 6) are indistinguishable at the 1 sigma level from the total fusion weighted mean age.

OTTB$_{total\ fusion}$: SUERC analysed 62 crystals of OTTB (sample NP9). Data define a weighted mean age of 785.7 ± 0.5/0.7 ka (Figure 5). No data points were rejected from the age calculation.

OTTB$_{step\text{-}heating}$: SUERC performed four step-heating experiments on four different aliquots of sanidine crystal populations (*n*3) (sample NP9). All experiments yielded 100% ^{39}Ar plateaux with initial $^{40}Ar/^{36}Ar$ trapped components that overlapped with atmospheric values (Lee et al., 2006). The weighted mean plateau age (785.3 ±

0.8/1.0 ka) and inverse isochron age (Figure 6) are indistinguishable at the 1 sigma level from the total fusion weighted mean age.

$MTT_{total\ fusion}$: SUERC analysed 83 crystals of MTT sanidine (sample NP2). The data show a bimodal distribution with an older age population of *c*. 800 ka (*n*33) and a juvenile population defining an age of 502.0 ± 0.6/0.7 ka (*n*50) (Figure 5). We consider the statistically significant juvenile population to define the age of the MTT eruption. Owing to the presence of xenocrysts we did not perform incremental step-heating on small crystal populations. Note the xenocryst age population is consistent with the approximate age of the OTT.

$BT_{total\ fusion}$: SUERC analysed 225 crystals of BT sanidine using a single mass spectrometer and BGC analysed 94 crystals using two different mass spectrometers with the samples irradiated in two separate batches. The data yielded a weighted pooled mean of 766.8 ± 0.4/0.6 ka (*n*319), with no data points rejected (Figure 7).

$BT_{step\text{-}heating}$: SUERC performed eight step-heating experiments on eight different aliquots of sanidine crystal populations (*n*3). All experiments yielded 100% ^{39}Ar plateaux with initial $^{40}Ar/^{36}Ar$ trapped components that overlapped with atmospheric values (Lee et al., 2006). The weighted mean plateau age (766.1 ± 0.6/0.8 ka) and inverse isochron age (Figure 7) are indistinguishable at the 1 sigma level from the total fusion weighted mean age.

$LCTB_{total\ fusion}$: SUERC analysed 34 sanidine crystals of LCTB. The data show a dominantly bimodal distribution with an older age population of *c*. 700 ka (*n*5) and a single old crystal of *c*. 960 ka (*n*1). 28 sanidine crystals defined a juvenile age population with weighted mean age of 627.0 ± 1.5/1.7 ka (Figure 8). We consider this juvenile age population to define the age of the LCTB eruption. Owing to the presence of xenocrysts we did not perform incremental step-heating experiments.

The *R*-values and their corresponding ages (calculated weighted averages for samples that have both fusion age and step-heating age data) are shown in Table 1

and appendix file 'SF#1' (.pdf). It is these ages (Table 1) and associated *R*-values that are discussed throughout the remainder of the text.

Discussion

$^{40}Ar/^{39}Ar$ dating of the proximal Toba Tuffs

We performed $^{40}Ar/^{39}Ar$ dating on sanidine separated from the proximal YTT, MTT, OTTA (Siguragura) and OTTB (Harrangoal) that have been correlated geochemically to tephra layers preserved within the marine core record to construct a high-precision radioisotopic chronology for the Pleistocene of ODP 758 that is independent of the astronomical age model.

The $^{40}Ar/^{39}Ar$ age data for the YTT (Ash A) have been published previously and define a robust inverse isochron age, the data being reported relative to the ACs standard age of 1.2056 Ma (Renne et al., 2011). This age for the YTT was indistinguishable from the YTT age of Storey et al. (2012), relative to the same $^{40}Ar/^{39}Ar$ calibration. Taking the new published optimisation model ACs age of Niespolo et al. (2016) into account, we have taken this opportunity to recalculate the ages of Mark et al. (2014) and Storey et al. (2012). This yields the most accurate and precise age for the YTT, integrating the data from both laboratories to give an age of 73.7 ± 0.3/0.4 ka (R_{ACs}^{YTT}: 0.06196 ± 0.00025). Note the recalculated data is available in appendix file 'MBB data summary' (.pdf). The age of the MTT (502.0 ± 0.6/0.7 ka, R_{ACs}^{MTT}: 0.42219 ± 0.00050) is in agreement with the $^{40}Ar/^{39}Ar$ age of Chesner et al. (1991) allowing for differences in the $^{40}Ar/^{39}Ar$ calibration used. Our data for the OTT show that at *c.* 800 ka there were two temporally distinct eruptions from the Toba volcano: OTTA and OTTB, 792.4 ± 0.5/0.6 ka (R_{ACs}^{OTTA}: 0.6646 ± 0.00042) and 785.6 ± 0.7/0.8 ka (R_{ACs}^{OTTB}: 0.66075 ± 0.00059), respectively. There is a *c.* 6 ka temporal

offset between these two eruptions, which broadly agrees with the temporal offset suggested by the application of the average ODP 758 sedimentation rate between Ash *d* and Ash D (discussed above). The age for Ash D is also indistinguishable from the astronomically tuned age presented by Lee et al. (2004) of 788.0 ± 2.2 ka. These two ages (our $^{40}Ar/^{39}Ar$ age and the astronomically calibrated age) are in good agreement with the previous OTT/Ash D $^{40}Ar/^{39}Ar$ age of Hall & Farrell (1995) but younger than the OTT $^{40}Ar/^{39}Ar$ age of Diehl (1987).

The geochronological data and reinterpretation of the field geology show that the proximal Toba stratigraphy requires further detailed mapping, geochemistry, and eruption volume estimates so that we can develop a revised understanding of the old Toba eruption cycle. Ash E in ODP 758 is geochemically distinct from any of the Toba eruption products that we have analysed and, at present, the tephra provenance is unknown.

A Bayesian $^{40}Ar/^{39}Ar$ age-depth model for the Pleistocene of ODP 758

Bayesian age-depth modelling of ODP 758 was performed using the OxCal (ver. 4.2) software of Bronk Ramsey et al. (2013). A '`P_Sequence`' (i.e., Poisson process) deposition model was applied (Bronk Ramsey, 2008), whereby the deposition rate of the sediment sequence is allowed to vary from that of a constant deposition rate through time (i.e., a uniform '`U_Sequence`' in OxCal) according to the additional constraint of a parameter, 'k' (a higher value of k gives an increasingly linear deposition rate; lower values of k allow increasing flexibility away from a uniform deposition rate). In the context of sediment deposition, the `P_Sequence` model provides a realistic representation of sediment accumulation, with the complexity (randomness) of the underlying deposition modelled according to a Poisson process. The k parameter is not fixed *a priori*, allowing the program itself to determine an unbiased measure of the rigidity of the deposition rate, based upon the dating

('likelihood') information combined within the P_Sequence model prior (Bronk Ramsey & Lee, 2013).

Since the four tephra layers within ODP 758 represent macroscopic, instantaneous deposits ('instantaneous' in the context of the timescales considered here, at least), their respective thicknesses (Ash A, YTT 34 cm; Ash V, MTT 23 cm; Ash d, OTTB 13 cm; and Ash D, OTTA 2 cm thick) were excluded to provide an 'event-free depth' scale (e.g., Katsuta et al., 2007; Schlolaut et al., 2012) so that the regular, 'background' deposition rate could be effectively modelled.

In addition to the four $^{40}Ar/^{39}Ar$ dated tephra units, 'Date' functions were also inserted within the model to provide posterior age distributions for the depths of the MBB, Australasian tektite layer, and Jaramillo event (onset and termination) within ODP 758 (unlike the tephra units, these latter Date functions were included without any prior chronological information associated with them). The top and bottom of the sediment sequence (at 0 and 18.9 m depth) were additionally constrained by 'Boundary' functions, with the upper boundary defined as the date of core extraction, AD 1988. The lower boundary was somewhat arbitrary, but represents the subsequent break between core sections below the Jaramillo event, the base of section 758B-2H (Shipboard Scientific Party 1989). As there was no other sedimentological evidence within the stratigraphy for abrupt changes in the mode of sediment deposition, no further 'Boundary' functions were inserted within the P_Sequence model.

To assess whether two age distributions are statistically different within OxCal, the 'Difference' function (which simply subtracts one age distribution from another) is applied. Here, Difference queries were applied between the modelled ODP 758 ages and published ages for both the MBB and Australasian tektite layer. If the calculated probability range for the Difference query does not include zero at a given confidence level (typically, 95.4% confidence), a null hypothesis (that the two

age distributions are consistent) can be rejected, and the ages can be described as being statistically significantly different (Macken et al., 2013; Wood et al., 2014).

Due to the limited number of likelihood data (i.e., four $^{40}Ar/^{39}Ar$ ages plus date of core extraction) within the model, there is no contradictory information (given the model prior) to 'pull' the modelled age-depth profile away from the raw, un-modelled data. Accordingly, all of the individual modelled data points exhibit excellent agreement indices of 100% (i.e., there is no evidence of stratigraphic inversions, or unreliable $^{40}Ar/^{39}Ar$ measurements.)

In order for the Poisson process (P_Sequence) age-depth profile to pass through these data points (which fall well away from linear sediment deposition), however, the modelled k parameter must be fairly low. The result of this is that the chronological precision of the interpolated (and extrapolated) depths is lower than if the deposition rate were more linear (i.e., if OxCal had determined a higher value for k). This reduction of modelled chronological precision becomes more pronounced further away from the $^{40}Ar/^{39}Ar$-dated core depths, as illustrated in Figure 9.

Table 2 provides a summary of unit/event depth information (both mbsl and 'event-free' depth) used in the model construction. Note that interpretation of the positions of geomagnetic events within marine cores can be subjective - we have used the depths for the tephra layers and geomagnetic polarity reversals that have been published previously (Dehn et al., 1991; Farrell & Janecek, 1991). We note that, unfortunately, paleomagnetic intensity data are not available for ODP 758 but, due to the sensitivity of the model to the $^{40}Ar/^{39}Ar$ data and large uncertainties as we move away from these tie points, small changes (i.e., cm-scale changes) in the location of the MBB will not significantly impact the age ranges reported relative to the uncertainty associated with each modelled age (median age shifts approximately 0.7 ka/cm).

ODP 758 defined MBB age

The modelled age for the MBB (all modelled ages below reported at the 68.2% confidence level) is 784 ± 2 ka (Figure 9). The MBB age as defined by ODP 758 is statistically older (at the 95.4% confidence level) than the proposed age of Channell et al. (2010) for the North Atlantic, but in complete agreement with the age proposed by Sagnotti et al. (2014) for samples from the Sulmona Basin. This age is indistinguishable from the ODP 758 astronomically tuned age of c. 784 ka.

ODP 758 defined JGE age

The modelled age range for the MBB is more precise than the extrapolated ages derived for the JGE_{onset} (median: 1,082 ka, 1,001-1,159 ka) and $JGE_{termination}$ (median: 1,002 ka, 933-1,064 ka) (Figure 9). This is due to the lack of an age constraint stratigraphically below the JGE within ODP 758 to anchor the Bayesian age-depth model. We are surprised however that even with absence of this constraint, that the median ages are relatively close to the reported ages for the onset (1070 ka) and termination (997 ka) of the JGE, respectively (Chen et al., 1995). With respect to current discussions in the literature (e.g., Singer, 2014) our data, owing to this low precision output from the model (i.e., lack of a temporal marker below the JGE_{onset}), do not advance understanding of the timing of the JGE.

The Age of the Bishop Tuff

A robust age for the BT will allow determination of a North American MBB age that provides an independent comparison with the ODP 758 constraint. New data collected here and re-calculation of previously published data (e.g., Simon et al., 2014) shows that there is temporal alignment between the $^{40}Ar/^{39}Ar$ and ^{238}U-^{206}Pb geochronometers for the BT. However, we suggest caution in the (over)interpretation

723 of the high precision zircon ID-TIMS ^{238}U-^{206}Pb ages for dating of Pleistocene
724 volcanic eruptions.

725 A 'high-precision' BT zircon ID-TIMS ^{238}U-^{206}Pb age of 767.1 ± 0.5 ka (1
726 sigma, full uncertainty, Crowley et al., 2007) is significantly younger than the BT
727 zircon ion microprobe (SIMS) ages (Reid & Coath, 2000; Simon & Reid, 2005) that
728 suggest a mean pre-eruptive zircon magma residence time greater than 50 ka.
729 Recently, Ickert et al. (2015) collected new SIMS and ID-TIMS ^{238}U-^{206}Pb age data
730 and demonstrated both inter- and intra-grain variability in apparent U-Pb ages of BT
731 zircon crystals. The new data support the forward modelling of Simon et al. (2008)
732 and explain the discrepancy when interpreting the previous SIMS and ID-TIMS U-Pb
733 age data (Reid & Coath, 2000; Simon & Reid, 2005; Crowley et al. 2007), but
734 highlight that the single coherent population of juvenile crystals dated by Crowley et
735 al. (2007) was not an 'eruption age' as previously implied, but a result of the strong
736 correlation of the uncertainty in one component of the ^{230}Th disequilibrium correction.
737 If the correlation is accounted for correctly then there exists substantial variability in
738 the ages of the zircon crystals that precludes determination of a meaningful weighted
739 mean crystallisation age.

740 The dating of BT zircon by U/Pb methods is highly challenging because the
741 concentration of radiogenic Pb is low and the correction required for disequilibrium in
742 the intermediate daughter products is large. These corrections for young zircon are
743 significant, for example, a correction of greater than 80 ka was employed previously
744 for BT zircon (Crowley et al., 2007). Moreover, the corrections are often based on
745 best-case scenarios and assumptions (models) that are difficult to validate, e.g., that
746 the host magma 'Th/U_{melt}' composition employed accurately represents the melt
747 composition from which the zircon grew and requires that the magma itself was in U-
748 series equilibrium prior to zircon growth. Hence the utmost caution must always be
749 employed when interpreting geologically young ID-TIMS ^{238}U-^{206}Pb BT zircon data

with respect to 'eruption ages' and we suggest that in general, such ages reported with relative uncertainties at the permil level are suspect of being unduly optimistic.

Several studies have now shown that young ID-TIMS ^{238}U-^{206}Pb zircon ages 'approach' eruption ages (e.g., Rivera et al., 2013), but as highlighted by Ickert et al. (2015) - when interpreting such data (i.e., zircon that forms/closes over a continuum rather than in response to a specific geological event, e.g., eruption) one should appreciate that employment of a weighted mean to geologically young high-precision zircon ages requires an assumption that necessitates a geologically implausible event. A further, important point to note is how the Th/U_{melt} uncertainty is propagated in the correction (e.g., Crowley et al. 2007). This also affects the reported uncertainty of the new zircon rim 'eruption age' measured by SIMS (Chamberlain et al., 2014; discussed in-depth by Ickert et al., 2015). For the uncertainty propagation two approaches are prevalent. The first is similar to that of Crowley et al. (2007). The Th/U_{melt} correction is applied to each individual zircon analysis and then the weighted mean of the population is determined. In the second the Th/U_{melt} is treated as a systematic variable, and so this uncertainty is propagated following determination of a weighted mean age, applying it to the weighted mean $^{206}Pb^*/^{238}U$. The latter leads to a larger and we contend a more realistic age uncertainty. Note that the uncertainty on the corrected age has an inverse relationship with the Th/U_{melt} value, which is clearly demonstrated in Figure 10.

Sarna-Wojcicki et al. (2000) presented the first 'high-precision' $^{40}Ar/^{39}Ar$ age measurements from the BT but recently the BT has been extensively studied. Rivera et al. (2011) reported an $^{40}Ar/^{39}Ar$ sanidine age of 767.4 ± 1.1 ka (R_{FCs}^{BT}: 0.02706 ± 0.00005), relative to their proposed astronomically tuned age for Fish Canyon sanidine (FCs). Zeeden et al. (2014) made measurements in the same laboratory and reported a BT $^{40}Ar/^{39}Ar$ age that is identical to the age reported by Rivera et al. (2011) but note they rejected more than 30 % of their data culling the MSWD to 0.3

777 to improve analytical precision. Although the data were trimmed symmetrically
778 around the determined mean (not impacting accuracy), this is an approach that is not
779 'best practice' with respect to statistical assessment of geochronological data.
780 Relative to the highest precision attainable using the $^{40}Ar/^{39}Ar$ technique, the data of
781 Sarna-Wojcicki et al. (2000), Rivera et al. (2011) and Zeeden et al. (2014) can be
782 improved on. Thus we collected new high-precision $^{40}Ar/^{39}Ar$ age data to better
783 define R_{ACs}^{BT} (Figure 7). Exhaustive new analyses validate the results of Rivera et al.
784 (2011) and Zeeden et al. (2014). However, for calculation of $^{40}Ar/^{39}Ar$ ages we do not
785 favour the use of the FCs calibration presented by Rivera et al. (2011); we provide
786 our reasoning below.

787 $^{40}Ar/^{39}Ar$ data (Renne et al., 2013) for the Cretaceous-Palaeogene (K-Pg)
788 boundary show that the orbitally-tuned FCs calibration of Rivera et al. (2011) places
789 the K-Pg boundary exactly intermediate between two possible choices of 405 ka
790 orbital eccentricity cycles. The implication is that the astronomically tuned age for
791 FCs (Rivera et al., 2011) is paradoxically inconsistent with any astronomically tuned
792 age for the K-Pg boundary. Rather the $^{40}Ar/^{39}Ar$ calibration (FCs age) of Renne et al.
793 (2011) is proven to be the most consistent with the orbitally-tuned age (Kuiper et al.,
794 2008) for the K-Pg boundary (Renne et al., 2013). It is this calibration with robust and
795 quantifiable uncertainties that we favour. Using the updated R_{FCs}^{ACs} (0.041707 ±
796 0.000011) reported by Niespolo et al. (2016) as a parameter in the optimized
797 calibration of Renne et al. (2010), along with the decay constant from Renne et al.
798 (2011), our $^{40}Ar/^{39}Ar$ data define a BT eruption age of 766.6 ± 0.4/0.5 ka (R_{ACs}^{BT}:
799 0.64473 ± 0.00034) (Figure 7).

800 In view of our comprehensive data set, from multiple eruptive BT units (*n*3),
801 laboratories (*n*2), mass spectrometers (*n*3), and operators (*n*3), we regard this as the
802 most precise and accurate age for the BT. The $^{40}Ar/^{39}Ar$ age of Rivera et al. (2011)
803 recalculated relative to the same parameters as our data is 767.6 ± 1.0/1.1 ka, the

$^{40}Ar/^{39}Ar$ age of Sarna-Wojcicki et al. (2000) is 768.7 ± 3.2/3.3 and the $^{40}Ar/^{39}Ar$ age of Simon et al. (2014) is 769.0 ± 3.1/3.2 ka. These data are all indistinguishable relative to each other and consistent with a relatively imprecise astronomically tuned age for the Bishop Tuff of 765 ± 8 ka (Zeeden et al., 2014). The data are also consistent with the interpretation of Ickert et al. (2015) that the BT zircon ID-TIMS ^{238}U-^{206}Pb eruption age is < 775 ka. Figure 11 shows a summary of these data against the 'weighted mean' BT zircon ID-TIMS ^{238}U-^{206}Pb age (Crowley et al., 2007) and the BT zircon ID-TIMS ^{238}U-^{206}Pb age distribution of Ickert et al. (2015).

The ^{238}U-^{206}Pb data, $^{40}Ar/^{39}Ar$ and astronomical ages have all converged for the BT, to provide a robust temporal marker for the Pleistocene Time Scale.

The MBB and the Bishop Tuff

To define the most accurate age for the North American MBB relative to the BT we adopted the same approach as Sarna-Wojcicki et al. (2000), but built in extra uncertainty to our calculations (as detailed below). We highlight that due to the nature of the terrestrial sections used by Sarna-Wojcicki et al. (2000) (potential for unknown hiatuses in the stratigraphy) this approach is not going to yield a high-precision age constraint, just a useful comparison with the ODP 758 and Channell et al. (2010) MBB ages.

We have made new $^{40}Ar/^{39}Ar$ age determinations on sanidine from the LCTB (Figure 8), the tuff that postdates the BT in several North American sections that also contain a record of the MBB position (Figure 12). Single crystal analyses show a LCTB juvenile age population (*n*28) with a robust $^{40}Ar/^{39}Ar$ age of 627.0 ± 1.5/1.7 ka (R_{ACs}^{LCTB}: 0.52734 ± 0.00126). Note that our age for the LCTB is indistinguishable from the $^{40}Ar/^{39}Ar$ age of Matthews et al. (2015) when both are calculated relative to the same calibration (627.4 ± 1.5/1.7 ka, R_{ACs}^{LCTB} 0.52754 ± 0.00124) and is also

831 indistinguishable at the 2 sigma confidence level from the ID-TIMS $^{206}Pb/^{238}U$ LCTB
832 age (629.2 ± 4.3 ka, 2 sigma full uncertainty) reported by Wotzlaw et al. (2015).
833 As the LCTB postdates the BT we then, following Sarna-Wojcicki et al.
834 (2000), simply calculated the sedimentation rate between LCTB and BT, and
835 subsequently extrapolated Δ*t* from the BT to the MBB in each (*n*5) individual section
836 (Figure 13, Table 3). As expected, there is considerable scatter in the extrapolated Δ*t*
837 and MBB ages (MSWD 54) relative to what precision would predict, due most likely
838 to the presence of hiatuses in the stratigraphic sections, either between the LCTB-BT
839 and/or BT-MBB. Therefore, we deem it inappropriate to use the standard error of the
840 mean as a representative uncertainty for the BT-defined MBB age constraint. We
841 choose to use the SEM×SQRT(MSWD) of all five measurements as the most
842 appropriate method for determining a robust uncertainty. Note that we assigned 20%
843 uncertainty to the stratigraphic distances between LCTB, BT and the MBB to also
844 account for potential hiatuses in the stratigraphy at each site (Table 3). The approach
845 defines a MBB age of 789.1 ± 5.6 ka (68.2% confidence). Simply using the average
846 age ± standard deviation of the stratigraphic and age measurements for each sites
847 yields an MBB age of between 776-802 ka (Table 3). Both age ranges are resolvable
848 from the proposed MBB age of Channell et al. (2010).
849
850 The age of the MBB
851
852 In proposing paradigm-changing shifts in the age of key events within the Geological
853 Time Scale the burden of proof is high. We feel that the data presented here, when
854 considered with respect to the study of Sagnotti et al. (2014), pose serious questions
855 concerning the accuracy of the approaches used previously to date the MBB (for
856 example: Channell et al., 2010). There are now three independent robust and
857 accurate $^{40}Ar/^{39}Ar$ age constraints indicating that current estimations for the age of
858 the MBB are too young. As such, the revision to the Geological Time Scale that we

propose has far reaching implications for Quaternary science and other dating techniques.

Taking the two MBB age constraints from this study (ODP 758 and LCTB-BT-MBB) and the MBB age of Sagnotti et al. (2014) we can calculate a weighted average MBB age: 783.4 ± 0.6 ka (R_{ACs}^{MBB} 0.65885 ± 0.00050) (1-sigma, full external precision, MSWD 0.8). We consider this to be currently the most accurate MBB age and the most robust temporal anchor for the Pleistocene Geomagnetic Time Scale. It is *c*. 10.4 ± 1.5 ka older than the MBB age proposed by Channell et al. (2010), and consequently *c*. 3.4 ± 0.7 ka older than the age of the MBB in the LR04 stack (Lisiecki & Raymo, 2005) (or as defined by Shackleton et al., 1990).

We note that our absolute age for the MBB is dependent on the specific $^{40}Ar/^{39}Ar$ calibration used, but the difference between employment of the Rivera et al. (2011) calibration and the use of Niespolo et al. (2016) with Renne et al. (2011) results in a MBB age difference of 0.3 ± 2.0 ka. Thus it is inescapable that there are discrepancies between the most precise $^{40}Ar/^{39}Ar$ ages and some (but not all, see discussion below) orbital tuning ages for the MBB.

Magnetic lock-in delay

It may be questioned whether the ODP 758 MBB age that we present (or the approach we have taken with respect to OPD 758) is biased by delayed acquisition of magnetic remanence (i.e., lock-in) in the sediment (Kent, 1973; Suganuma et al., 2011), owing to a relatively low sedimentation rate. The only possible evidence for this is that the MBB in ODP 758 is not located at the same position within MIS 19 as it is in the high-resolution North Atlantic cores (Channell et al., 2010). There is no doubt that magnetic lock-in delay is a real issue for interpretation of paleomagnetic data from some sediment cores (e.g., Tauxe, 1996) but not others (e.g., Valet et al.,

886 2014) and that when assessing such phenomena, we have to consider the level of
887 precision one is achieving when temporally resolving paleomagnetic events relative
888 to any potential lock-in offset.

889 Typically, the degree of magnetic lock-in delay in marine sediments at the
890 depth of the MBB is minimal (e.g., Tauxe et al., 1996; Bleil & von Dobeneck, 1999;
891 Horng et al., 2002) but in ODP 758 we do not consider lock-in of paleomagnetic
892 remanence as significant, certainly at the depth of the MBB. Our reasoning for this is
893 that there are now three unrelated $^{40}Ar/^{39}Ar$ age constraints for the MBB from three
894 geographically distal sites representing three distinct depositional environments
895 (Sulmona Basin, North America, South China Sea) that are indistinguishable from
896 each other at the 68.2 % confidence interval. They yield a weighted mean MBB age
897 with a MSWD of 0.8, revealing no excess scatter in the data as there would be, for
898 example, if paleomagnetic lock-in delay was significant in one of the records. To
899 make an argument for our ODP 758 data being affected significantly by delayed
900 magnetic lock-in would require for the North America MBB record and the Sulmona
901 Basin record to be as equally offset from a younger MBB by exactly the same
902 amount of time. As a consequence, our data now raise two important questions: (1)
903 why is there an offset in the location of the MBB relative to MIS 19 in different
904 records? And (2) why are some orbitally tuned ages for the MBB consistently
905 younger than the most precise and accurate $^{40}Ar/^{39}Ar$ ages?

906

907 Why is there an offset in the location of the MBB relative to MIS 19?

908

909 As paleomagnetic lock-in delay in ODP 758 is not significant with respect to the
910 temporal resolution we have achieved, we are left with two possibilities to explain the
911 differences in the ODP 758 MBB location within MIS 19 relative to the high-resolution
912 North Atlantic cores (Channell et al., 2010): (i) it is the position of the MBB that has
913 changed within rock archives across the globe - diachronous onset as suggested by

914 previous modeling of the MB-reversal (Leonhardt & Fabian, 2007; Olson et al.,
915 2011); or (ii) it is not the position of the MBB that has changed, it is the onset and
916 termination of MIS 19 within marine records that are different across the globe
917 (relative to a fixed position for the geomagnetic reversal).

918 (i) As Earth's magnetic field intensity drops to low values during polarity
919 reversals the field direction progresses through a 180° change while the field is
920 weak. The time it takes for this process to happen is uncertain. Modeling of the MBB
921 event has suggested reversal durations of between 2-10 ka and highlighted potential
922 for a millennial-scale variability in onset of the MB-reversal for sites in the Atlantic
923 and Pacific Oceans (Leonhardt & Fabian, 2007). Such age offsets have not been
924 reported in the literature, although few existing age data are sufficiently precise to
925 resolve diachrony at this scale. A diachronous MBB is supported by the work of
926 Olson et al. (2011) who compared the MBB paleomagnetic trajectories to a complex
927 dynamo model depicting a polarity reversal. Both were initiated by gradual reductions
928 in dipole intensity leading to a reversal precursor event (intensity low) and
929 subsequent transient polarity recovery. Following this was rapid dipole collapse and
930 final directional reversal that began with reverse flux generation in one hemisphere.
931 Virtual geomagnetic poles (VGPs) from sites located proximal to the reverse flux
932 follow complex paths crossing the equator several thousand years prior to the
933 simpler VGP paths from the more distal sites – the magnetic intensity variations
934 produced by the dynamo model reversal correlate with intensity variations inferred for
935 the MBB (Olson et al., 2011).

936 These theoretical/model data suggest diachronous onset of the MB-reversal
937 on a time scale that should be resolvable using high-precision radio-isotopic dating.
938 However, our data show temporal coincidence of the MBB at the 68.2 % confidence
939 interval for three sites that vary with respect to latitude and longitude. Clement (2004)
940 noted that polarity reversal durations vary with site latitude; low latitude sites have
941 shorter reversal durations than mid- to high-latitude sites. As such, the physical data

(analytical measurements) do not appear to support a diachronous MB-reversal model (Leonhardt & Fabian, 2007; Olson et al., 2011) in which the reversal timing is a systematic function of latitude. Instead, the data support the interpretation that the MB-reversal was a globally isochronous event at the millennial scale.

(ii) Benthic $\partial^{18}O$ (e.g., Figure 14) is used to align marine records from across the globe. Simplistic tuning of records, or wiggle matching, requires one to make the assumption that the global climate system responds uniformly over millennial time scales. $\partial^{18}O$ change is thought generally to be globally synchronous to within 1 ka – the approximate mixing time of an ocean. This is the fundamental assumption in construction and utillisation of global marine stacks such as LR04 (Lisiecki & Raymo, 2005). Radiocarbon data support this supposition with ^{14}C ages of the Last Glacial Maxima as identified in $\partial^{18}O$ data agree to within 1 ka (Duplessy et al., 1991). If $\partial^{18}O$ changes are not synchronous to within the time it takes the oceans to mix, then any age model that is based on alignment of $\partial^{18}O$ signals would contain significant errors (several ka).

High-resolution records from the Iberian Margin that chart the last glacial termination (Termination I) provide direct evidence for diachronous benthic $\partial^{18}O$ response with ^{14}C age models showing the Atlantic was leading the Pacific by *c.* 4 ka (Skinner & Shackleton, 2005). The *c.* 4 ka offset would result in an erroneous age model if a stack was constructed or if benthic $\partial^{18}O$ was used as a proxy for ice volume. The mixing of $\partial^{18}O$ throughout the oceans is complicated further by changes in water depth. Studies have demonstrated that it can take an extra 1.5 ka for changes in $\partial^{18}O$ to reach deep-water sites within the same ocean (Labeyrie et al., 2005; Waelbroeck et al., 2006), let alone for $\partial^{18}O$ to be transmitted between shallow and deep water at sites more distal or isolated from the Atlantic.

Lisiecki & Raymo (2009) compared $\partial^{18}O$ records from both sites in the Atlantic and Pacific to assess the respective leads and lags in benthic $\partial^{18}O$. They concluded that $\partial^{18}O$ data show a statistically significant Atlantic lead relative to the

970 Pacific $\partial^{18}O$. For Terminations I-IV a Pacific benthic $\partial^{18}O$ lag of 1.6 ka was estimated
971 and at 128 ka and 330 ka, a *c.* 4 ka lag for the Pacific was determined. It was
972 concluded that such leads-lags, probably generated by diachronous temperature
973 changes (without the requirement for slower circulation), will lead to uncertainties of
974 several ka during glacial terminations and this must be taken in to account when
975 using benthic $\partial^{18}O$ records as a proxy for the timing of ice volume change. Lisiecki &
976 Raymo (2009) note that for different terminations the $\partial^{18}O$ lag could vary dramatically
977 due to the differences in ice volume at the glacial maximum and/or the insolation
978 forcing (Parrenin & Pailard, 2003; Parrenin et al., 2007). Given the increase in lag
979 times between the Atlantic and Pacific Oceans from 1.6 to 4 ka between
980 Terminations I-IV (20-330 ka) it is currently unclear what the lag time would have
981 been by Termination IX, the termination that pre-dates the MBB (Figure 14).

982 These data (Skinner & Shackleton, 2005; Lisiecki & Raymo, 2009) show that
983 the onset and termination of Marine Isotope Stages across the globe cannot, and
984 should not, be considered as synchronous at the level of temporal resolution now
985 attainable using radioisotopic dating. It is also unclear whether we can expect the
986 duration of MIS within different oceans to be the same or whether contraction-
987 expansion of MIS can occur, especially for sites that are proximal or distal to the sites
988 of ice melting (the poles). It is currently impossible to determine accurate age offsets
989 for the MIS times scale between the Atlantic and Pacific, let alone temporally
990 constrain interactions between the Atlantic and other oceans (e.g., Indian Ocean).

991 Therefore, we contend that within $\partial^{18}O$ records that are obtainable for the
992 Pleistocene there is no requirement for the position of the MBB to be located at the
993 same point in MIS 19. The fact that ODP 758 $\partial^{18}O$ data show the MBB at an earlier
994 position (Figure 2) in MIS 19 relative to the high-resolution records of the North
995 Atlantic (Channell et al., 2010) should not result in immediate dismissal as evidence
996 of a paleomagnetic 'lock in' delay (Roberts & Winklhofer, 2004; Suganuma et al.,

997 2011). Further, such $\partial^{18}O$ offsets between marine records should not be used as an
998 assessment of the degrees of paleomagnetic lock-in delay (e.g., Horng et al., 2002).
999 The EU-funded INTIMATE (INTegrating Ice core, MArine and TErrestrial
1000 records) network has recognized previously problems of assuming synchronous
1001 global response in climate systems and as such, has devised protocols to avoid
1002 making such assumptions, which can introduce unquantifiable uncertainties in age
1003 models (http://cost-es0907.geoenvi.org). INTIMATE correlations are based on
1004 independent tie-points (temporal anchors), which are coupled and compared through
1005 the use of either tephra markers (tephrochronology) (e.g., Smith et al., 2013) or
1006 accurate/precise chronologies (e.g., Smith et al., 2011; Staff et al., 2013). This
1007 approach has led to construction of robust 'event stratigraphies' that have allowed
1008 testing of leads and lags in response to climate forcing (Björck et al., 1998; Alloway
1009 et al., 2007). For 'absolute' dating of processes and events within the Geological
1010 Time Scale the INTIMATE approach is more robust than wiggle matching that, at
1011 best, allows for relative assessments of time.
1012
1013 Integration of the astronomical and $^{40}Ar/^{39}Ar$ MBB age
1014
1015 The new age for the MBB is consistent with the astronomical age reported by Chen
1016 et al. (1995) for ODP 758. At first sight there appears to be an offset between the
1017 MBB age obtained by us using the $^{40}Ar/^{39}Ar$ dating technique and the LR04 stack
1018 MBB age (Lisiecki & Raymo, 2005 and consequently the astronomical age of
1019 Shackleton et al., 1990). However, we do not consider this to be the case - with
1020 application of appropriate uncertainties (± 5 ka, Martinson et al., 1987) these ages
1021 are indistinguishable. We therefore propose our MBB age could now be used as a
1022 high-precision tie point in the model of Lisiecki & Raymo (2005) to line up the
1023 occurrence of the MBB in marine records that do not exhibit significant magnetic
1024 lock-in effects.

However, the offset with the proposed MBB age of c. 773 ka is real and we suggest there must be uncertainties (beyond reported precision) or errors in the approach of Channell et al. (2010). A detailed review and assessment of astronomical dating and its inherent uncertainties is beyond the scope of this contribution, but we can make some first order observations and pose questions for consideration.

We have already highlighted that previous work has suggested that any astronomically tuned age for the Pleistocene cannot be defined better than to within ± 5 ka (Martinson et al., 1987; Imbrie & Imbrie, 1980). Astronomical ages are derived by wiggle matching climate proxy cycles in sedimentary sequences to either: (1) astronomic solutions (Laskar, 2004) for orbital cycles, or (2) calculated solar insolation for a specific latitude and time of year (Milankovitch, 1930; Hays et al., 1976). For example, Figure 14 shows the planktonic and benthic $\partial^{18}O$ records for ODP 983 relative to ice volume models based on midsummer and integrated summer insolation forcing. If current levels of uncertainties associated with the astronomical dating approach are robust (Martinson et al., 1987), the revision we are proposing (c. 10 ka) to the astronomical MBB age (773 ± 1 ka) of Channell et al. (2010) (relative to our $^{40}Ar/^{39}Ar$ MBB age, 783.4 ± 0.6 ka) is too large to be accounted for by uncertainties in phasing assumptions. Whilst it is true that there are inherent uncertainties associated with the orbital calculations themselves; the orbital solution being sensitive to both shifts in tidal dissipation, and changes in global ice volume that may potentially alter the Earth's dynamical ellipticity (Laskar et al., 1993), other astronomical tuning studies (e.g., Shackleton et al., 1990; Chen et al., 1995) that report MBB ages indistinguishable from our MBB age, use the same orbital calculations which must have the same intrinsic uncertainties. The remaining possibilities are: (1) orbital sediment cycles may have been mis-mapped onto orbital forcing by Channell et al. (2010), or (2) the level of precision attained by Channell et al. (2010) is grossly underestimated. It should be noted that although Channell et al.

(2010) proposed an error of just ± 1 ka for their MBB age, this represents the standard deviation of the midpoint of the MB-polarity transition for multiple marine records, and not a realistic uncertainty associated with the astronomical dating approach to deriving the MBB age in the Atlantic marine cores.

The MBB and transitionally magnetized lava flows

As discussed above, $^{40}Ar/^{39}Ar$ ages for transitionally magnetised lava flows have been cited (Baksi et al., 1992; Singer & Pringle, 1996; Coe et al., 2004; Singer et al., 2005; Singer, 2014) as supporting evidence for the astronomical age of the MBB (Channell et al., 2010) and as evidence for a MBB precursor event. There are relatively large age corrections associated with the analysis of low radiogenic ^{40}Ar basaltic-andesitic groundmass that can significantly impact the accuracy of $^{40}Ar/^{39}Ar$ ages (McDougall & Harrison, 1999; Barfod et al., 2014). In comparison to the levels of precision achieved by Sagnotti et al. (2014) and here by the targeting of K-rich sanidine, the level of accuracy and precision attained for dating of young lavas is typically poor, especially if relying on high background isotope extraction techniques such as furnace step-heating (e.g., Singer et al., 2005).

Figure 15 shows the MBB lava data (Baksi et al., 1992; Singer & Pringle, 1996; Coe et al., 2004; Singer et al., 2005) relative to the proposed ages for the MBB. Note that none of the data are consistent with a MBB age of *c*. 773 ka (Channell et al., 2010) – this observation is independent of which $^{40}Ar/^{39}Ar$ calibration is utilised. Further, whereas it was previously concluded that the data from Chile, Tahiti and La Palma were dating a MBB precursor event, Figure 15 shows that these data are consistent with our ages for the MBB and the data of Sagnotti et al. (2014). In actual fact, we suggest that the data of Singer et al. (2005) are not dating two events (a MBB precursor event and the MB-reversal) as invoked previously to

explain the excess scatter in the data; the data are only dating the MB-reversal, albeit at relatively low accuracy and precision.

The large degree of scatter in data is probably associated with difficulty in dating basaltic-andesitic lava flows. For example, just by examining the data presented from Tahiti (Singer et al., 2005) atmospheric argon contamination ($^{40}Ar_{ATM}$) was accounting for (typically) more than 70 % of the total ^{40}Ar budget and thus any small error in this correction would impact age accuracy (but not necessarily age precision). In comparison to sanidine of similar age that we have dated, crystals typically contained *c.* 10% $^{40}Ar_{ATM}$. Hence the corrections are much smaller and easier to make. Most of the single data points of Singer et al. (2005), with the exception of some of the Maui data, are indistinguishable at 95% confidence from the MBB ages at 783.4 ± 0.6 ka when normalized to the same calibration (Figure 15). With respect to Figure 15 it is the Maui data although they could be dating the end of the MBB transition (we consider this unlikely given the reproducible MBB ages between sites of different latitudes and longitudes but the reversal duration is an important factor), they are most likely problematic (inaccurate), certainly at the levels of accuracy and precision that have been reported previously (Singer et al., 2005). Taking this in to consideration we have calculated a weighted average for all the ages for the MBB related lavas (including data from Maui) presented by Singer et al. (2005). We have determined the uncertainty using SEM×SQRT(MSWD) as there is significant scatter in the data (MSWD 7). The resultant age of 779 ± 7.5 ka (1 sigma, full external precision) is indistinguishable from the MBB age we present (783.4 ± 0.6 ka) as well as the astronomically tuned MBB age of 780 ± 5 ka (Lisiecki & Raymo, 2005).

It is important to note that we have not stated that there was not a MBB precursor event, as indeed different records highlight a geomagnetic intensity low prior to the MBB (Kent & Schneider, 1995; Hartl & Tauxe, 1996; Channell et al., 2009, 2010). We are simply stating that the $^{40}Ar/^{39}Ar$ data of Singer et al. (2005) are

1108 most likely associated with and dating the MBB. Apart from the age discrepancy
1109 reported by Singer et al., (2005) and the explanation invoked to explain this
1110 discrepancy, there is no paleomagnetic evidence that the lavas from these sites are
1111 related to a MB-reversal precursor event. In fact, the sites were specifically targeted
1112 in the first place as they were thought to contain detailed records of the MBB.
1113
1114 Implications for Quaternary age models
1115
1116 Decoupling the age of the MBB from the astronomical time scale and assumptions
1117 concerning alignment of $\partial^{18}O$ isotope records allows for independent testing of
1118 different Quaternary age models. It is important to realise that our results do not
1119 relocate the MBB within the different paleoclimate records; they simply question the
1120 robustness/accuracy of the time scales associated with the paleoclimate records.
1121 Termination IX within ODP 758 is coincident with OTTB at 785.6 ± 0.7/0.8 ka
1122 (Figure 2). Valet et al. (2014) using an astrochronological model determined a
1123 Termination IX age of 788-789 (± 5) ka from high-resolution Be records across the
1124 equatorial Indian Ocean, which allowing for the uncertainties associated with the
1125 astronomical tuning approach, is indistinguishable from the ODP 758 age. Further,
1126 as Valet et al. (2014) conducted both Be and paleointensity measurements on the
1127 same samples we can compare the age of the MBB in ODP 758 with the onset of the
1128 MBB from their study. Based on the astronomical age model presented by Valet et
1129 al. (2014) the relative paleointensity drop and recovery associated with the MBB
1130 occurred at 784 (± 5) ka while the cosmogenic Be data indicates reversal onset at
1131 780 (± 5) ka - both these ages for the MBB are indistinguishable from our reported
1132 MBB age of 783.4 ± 0.6 ka. These data are also commensurate with the age for
1133 Termination IX in the LR04 stack (788-789 (± 5) ka, Lisiecki & Raymo, 2005),.
1134 In addition to now having three independent radioisotopic age constraints
1135 (ODP 758, North America sections, Sagnotti et al., 2014) placing the MBB at 783 ±

0.6 ka, the MBB age reported by us is indistinguishable with the astronomical MBB age reported by Shackleton et al. (1990), Chen et al. (1995) Lisiecki & Raymo (2005) and Valet et al. (2014). The implication is that the MB reversal was, at the current levels of temporal resolution, isochronous. There is also agreement between all these records for the age of Termination IX. Our Termination IX age (785.6 ± 0.7/0.8) is also indistinguishable from the age for Termination IX as determined from the Sulmona Basin record (c. 787 ± 2/2 ka) (Giaccio et al., 2015).

Figure 14 (lower x-axes) shows that the offset between the onset of the MB reversal in the Atlantic Ocean record ODP 983 (Channell et al., 2010) and Termination IX is *c*. 15 ka (Channell et al., 2010). Accepting that the MBB age of Channell et al. (2010) is inaccurate and that the age presented here is correct, as well as assuming that the location of the MBB in the Atlantic records is accurate, then relative to a MBB age of c. 783 ka Termination IX in the Atlantic Ocean should be positioned at c. 798 ka. Does this observation suggest that with respect to the onset of Termination IX, the Atlantic Ocean was leading the Indian Ocean (and terrestrial records) in $\partial^{18}O$ response by *c*. 12 ka?

As discussed previously, Raymo (2009) did note that for different terminations the $\partial^{18}O$ lag does vary dramatically due to the differences in ice volume at the glacial maximum and/or insolation forcing (Parrenin & Pailard, 2003) with differences of ± 4 ka by Termination IV at 330 ka. If so, then this study and such a large lead-lag between the Atlantic and Indian Oceans further highlights that the dangers of 'wiggle matching' approaches to comparing climate records from across the globe.

We can also use the position of the 'isochronous' MB reversal within multiple paleoclimate archives to correlate between records. Raisbeck et al. (2007) concluded that the enhanced ^{10}Be flux in the EPICA Dome C ice core is a product of low dipole intensity during the MB-transition. Figure 16 shows the MBB tie point in different records at *c*. 783 ka allowing for correlation between the LR04 stack and EPICA Dome C, as well as correlation to Northern Hemisphere July insolation. The

horizontal displacement (along the x-axes) of these tie points shows the inaccuracies in the different time scales currently in use. Our interpretation does not impact the relative temporal offset within a single record, but does highlight that without high-precision independently dated tie points, it is currently not possible to directly compare climatic records from different sources throughout the Pleistocene.

The MBB has also been identified within Chinese loess and red clay sections (Zhou et al., 2014; Wang et al., 2014) but the apparent timing and duration of the MBB remain controversial due to inconsistencies in stratigraphic location. This Chinese record however is of key importance, as it would allow for cryospheric-marine-land correlation of climate records and paleoclimatic reconstruction across reservoirs. If as suggested (Zhou et al., 2014), S7 and S8 within the Chinese loess sections (Figure 16) correspond to MIS 19 and 21, respectively, then the MBB in the loess significantly pre-dates the MBB elsewhere. Complex post-depositional processes have been invoked to explain the massive downward shift of the MBB in the loess (Suganuma et al., 2010, 2011) but there is another possibility to consider. Several studies have previously proposed that S8 correlates to MIS 19 (Liu et al., 2008; Yang et al., 2010; Wang et al., 2006; Jin & Liu, 2011) and not MIS 21, which then places the MBB in the Chinese loess sections close to the location of the MBB in both the marine records and ice cores. Although this interpretation causes issues for stratigraphic correlation between the loess sections in China (Zhou et al., 2014), we consider it to be the most plausible with respect to the evidence at hand. Figure 16 shows the proposed correlation and the linkage of S8 to MIS 19.

ODP 758 defined Australasian Tektite age

The modelled mean age for the Australasian tektite layer (main concentration interval in ODP 758) is 786 ± 2 ka (Figure 9). The stratigraphic position pre-dates Termination IX, which is positioned at 785.6 ± 0.7/0.8 ka and we consider this

1192 modelled age to currently be the most accurate age for the tektites. As the
1193 Australasian tektites are found in Indochina, southern China, the Philippines,
1194 Malaysia, Indonesia and Australia an accurate age could be used as an isochronous
1195 marker horizon across continents (Smith et al., 2011, 2013). In the absence of a
1196 crater location, it has been suggested that the impact event that produced the tektites
1197 is located in Indochina, probably in close proximity to ODP Hole 1144A (Glass &
1198 Koeberl, 2006), but this remains supposition.
1199
1200 Conclusions
1201
1202 The present study has (1) provided a robust chronology for the multiple
1203 eruptions of the Toba super-volcano, (2) identified a multiple Toba eruption scenario
1204 at approximately 800 ka, (3) provided a robust and accurate age for the Australasian
1205 tektites, (4) defined robust high-precision ages for the BT and LCTB, (5) allowed for
1206 determination of an accurate and precise MBB age of 783.4 ± 0.6 ka, (6) shown at
1207 the level of temporal resolution attainable using radioisotopic dating the MB reversal
1208 can be considered isochronous, and (6) dated Termination IX in in the Indian Ocean.
1209 We highlight issues that pose significant challenges to the accuracy of U/Pb zircon
1210 dating in the Quaternary and suggest that relative uncertainties at the permil level are
1211 unduly optimistic. Finally, at the level of resolution now attainable for Pleistocene
1212 climate archives using radioisotopic dating, it is not valid to assume that response to
1213 changing $\partial^{18}O$ can be considered synchronous.
1214 As ODP 758 features in the LR04 marine stack, the high-precision $^{40}Ar/^{39}Ar$
1215 ages for the YTT, MTT, OTTA and OTTB, as well as the age for the MBB and
1216 Australasian tektites, can be used as temporally accurate and precise anchors.
1217 These anchors allow for global-correlation of the geological record, synchronisation
1218 of $\partial^{18}O$ climate archives (e.g., ice cores, lake records and speleothems) (e.g., Mark et
1219 al., 2014), and for testing of the inter-hemispheric phasing of climate (Shulmeister et

al., 2006; Broecker, 1998; Stocker & Johnsen, 2003; Mark et al., 2014). If the misalignment of the Chinese loess sequences is, as suspected, responsible for placing the MBB relative to MIS 19 in the wrong place, then the MBB tie point can, for the first time, allow for climatic reconstruction and correlation within different paleoclimate archives.

ACKNOWLEDGEMENTS

DFM thanks NERC for continued funding of the Argon Isotope Facility at SUERC and NERC Faciltiies grant IP/1626/0516. PRR thanks the Ann and Gordon Getty Foundation and the U.S. National Science Foundation (grant BCS-0715465) for support of his work. LM was funded by the Marie Curie FP7 Intra-European Fellowship Program for the duration of this project. VCS acknowledges support from the John Fell Fund, University of Oxford. Nick Pearce is thanked for providing samples of the Toba eruptions. Al Deino and Klaudia Kuiper are thanked for fruitful discussion and input to the study. Brad Singer, Matt Heizler, Mike Storey and Tiffany Rivera are thanked for discussion concerning the age of the Bishop Tuff and the MBB. Jim Channell is thanked for discussion of MBB timing as recorded in the marine realm. Jim Imlach is thanked for technical assistance. Two reviewers are thanked for detailed comments that have led to significant improvement of this manuscript. Any use of trade, product, or firm names is for descriptive purposes only and does not imply endorsement by the U.S. Government.

FIGURE CAPTIONS

1246 Figure 1: (A) World map showing the locations of marine cores referred to in main
1247 text. (B) Map showing location of ODP 758 relative to Sumatra and Toba as well as
1248 the known distribution of Toba eruptive deposits throughout the region (green dots).
1249
1250 Figure 2: Composite core for ODP 758 (Farrell & Janecek, 1991) showing (i)
1251 composite magnetic stratigraphy (declination) for ODP 758, (ii) Magnetic
1252 susceptibility for ODP 758 with the locations of the Ashes A, C, D and d (i.e.,
1253 correlated Toba Tuffs), and (iii) the geomagnetic timescale. Planktic and Benthic
1254 foraminifera $\partial^{18}O$ records for ODP 758 composite are shown highlighting the position
1255 of the MBB within Marine Isotope Stage 19. The orange line (coincident with Ash D)
1256 shows the position of Termination IX within ODP 758.
1257
1258 Figure 3: Map showing the location of sampling sites relative to the Toba Caldera
1259 with the respective stratigraphies for both sites. Further details on the stratigraphic
1260 sequences are provided in the text.
1261
1262 Figure 4: Glass and biotite geochemistry for ODP 758 Ashes D, d and E as well as
1263 proximal YTT, MTT and OTT data from Siguragura and Harrangoal. Note the glass
1264 geochemistry cannot distinguish between the data from the YTT and OTT deposits,
1265 but the biotite shows a definitive correlation with the OTT. Ash E was distinctly
1266 lacking in biotite, only one crystal was found.
1267
1268 Figure 5: $^{40}Ar/^{39}Ar$ single crystal fusion data for the MTT, OTTA and OTTB.
1269
1270 Figure 6: Incremental step-heating $^{40}Ar/^{39}Ar$ age spectra and isotope correlation plots
1271 (OTTA and OTTB).
1272

Figure 7: $^{40}Ar/^{39}Ar$ single crystal fusion data and incremental step-heating age spectra and isotope correlation plots for Bishop Tuff sanidine.

Figure 8: $^{40}Ar/^{39}Ar$ single crystal fusion data for LCTB.

Figure 9: Bayesian age-depth model for ODP 758. Anchor points shown in black and model outputs shown in red. The horizontal bars beneath each probability distribution, and the interpolated blue probability envelope represent the 68.2% confidence level.

Figure 10: Plot showing how the estimated Th/U_{melt} composition affects the re-calculated ID-TIMS U-Pb zircon 'eruption' age (black circle) of Crowley et al. (2007) (*n*17/19). The Th/U_{melt} is treated as a systematic variable, and so this uncertainty is propagated following determination of the weighted mean age. Uncertainty envelopes are shown for the Th/U_{melt} range (± 0.16) used by Crowley et al. and a 'more credible' Th/U_{melt} range (± 0.60) that reflects *c*. 68% of the variability seen in BT pumice and/or melt inclusions. Of note is the fact that the $^{40}Ar/^{39}Ar$ Bishop Tuff age reported in this study is consistent with the ID-TIMS U-Pb zircon age regardless of what Th/U_{melt} composition is assumed. Note all ages are shown including full external uncertainties and are displayed at the 2-sigma confidence level.

Figure 11: Geochronological summary plot for the Bishop Tuff. The $^{40}Ar/^{39}Ar$ data of Sarna-Wojcicki et al. (2000), Rivera et al. (2011) and Simon et al. (2014) are shown relative to the BT $^{40}Ar/^{39}Ar$ age presented here. The data are plotted relative to the BT astronomical age of Zeeden et al. (2014) and the ID-TIMS $^{206}Pb/^{238}U$ zircon ages of Ickert et al. (2015). The data are corrected for Th/U_{melt} using a value of 2.81 (Anderson et al., 2000) – the data cannot be interpreted with respect to a mean age as each bulk zircon age is a function of integrating a time-series of crystallisation.

1301 Ickert et al. (2015) highlight that with a Th/U_{melt} value of 2.81 the BT probably erupted
1302 post-775 ka (blue line in figure). For illustration purposes we have shown the
1303 $^{206}Pb/^{238}U$ age reported by Crowley et al. (2007) but see main text for comments
1304 concerning use of this 'weighted mean' age.
1305
1306 Figure 12: (A) Map showing region of LCTB-BT-MBB study sites in North America.
1307 (B) Location of specific study sites.
1308
1309 Figure 13: Schematic drawing showing the relationship between the BT, LCTB and
1310 MBB in North America. The symbols correspond to the calculations shown in Table
1311 3.
1312
1313 Figure 14: Plot showing the record for both benthic (grey) and planktic (black) $\partial^{18}O$
1314 from ODP 983 (adapted from Channell et al., 2010). Also shown is Virtual
1315 Geomagnetic Polar (VGP) latitude (black) and relative intensity proxy (grey). Ice
1316 volume models based on midsummer (orange) and integrated summer (blue)
1317 insolation forcing are also plotted. The blue line shows the position of the MBB in the
1318 records and the blue box the duration of the MB-reversal at the site of ODP 983 as
1319 defined by the benthic $\partial^{18}O$. The lower x-axis shows the astronomical timescale as
1320 discussed by Channell et al. (2010 whereas the upper x-axis shows the revised
1321 chronology based on the high precision $^{40}Ar/^{39}Ar$ age constraints presented here.
1322
1323 Figure 15: Plot showing age of transitionally magnetised lava flows (Baksi et al.,
1324 1992; Singer & Pringle, 1996; Singer et al., 2005) relative to Renne et al. (2011) and
1325 the MBB ages for ODP 758, North America, Sulmona Basin (Sagnotti et al., 2014)
1326 and the estimated MBB age of Channell et al. (2010).
1327

Figure 17: Plot showing the MBB tie points in multiple records (LR04, Antarctic Ice Core, Chinese Loess Stack) relative to Northern Hemisphere July insolation. Given the lack of evidence for diachronous onset the MBB should be the same age in all records. The upper x-axis shows the newly $^{40}Ar/^{39}Ar$ anchored time scale. Marine Isotope Stages, Glacial Terminations and Chinese loess paleoclimate and paleomagnetic records are all displayed.

Supplementary information (SF#) is presented as a PDF file

- SF#1 (.pdf): Geochem. summary (microprobe analyses) and MBB data summary ($^{40}Ar/^{39}Ar$ data).

References

Alloway, B.V., Lowe, D. J., Barrell, D. J. A., Newnham, R. M., Almond, P. C., Augustinus, P. C., Bertler, N. A. N., Carter, L., Litchfield, N. J., McGlone, M. S., Schulmeister, J., Vandergoes, M. J., Williams, P. W. and NZ-INTIMATE members., 2007. Towards a climate event stratigraphy for New Zealand over the past 30 000 years (NZ-INTIMATE project). *Journal of Quaternary Science*, 22 (1), pp. 9–35.

Anderson, A.T., Davis, A.M. & Lu, F.Q., 2000. Evolution of Bishop Tuff rhyolitic magma based on melt and magnetite inclusions and zoned phenocrysts. *Journal of Petrology*, 41 (3), pp. 449–473.

Baksi, A.K., Hsu, V., McWilliams, M. O. and Farrar, E., 1992. $^{40}Ar/^{39}Ar$ dating of the Matuyama-Brunhes geomagnetic field reversal. *Science,* 256 (5055), pp. 356-357.

1354 Barfod, D.N., Mark, D. F., Tait, A., Dymock, R. C., Imlach, J., 2014. Argon extraction
1355 from geological samples by CO_2 scanning laser step-heating. *Geological Society,*
1356 *London, Special Publications*, 378 (1), pp. 79–90.

1357 Berger, A.L. and Loutre, M.F., 1988. New insolation values for the climate of the last
1358 10 million years. *Sc. Report 1988/13 Institut d'Astronomie et de Géophysique G.*
1359 *Lemaître,* Université Catholique de Louvain, Louvain-la-Neuve.

1360 Bjorck, S., Walker, M.J.C., Cwynar, L.C., Johnsen, S., Knudsen, K-L., Lowe, J.J. &
1361 Wohlfarth, B., 1998. An event stratigraphy for the last termination in the North
1362 Atlantic region based on the Greenland ice-core record: a proposal by the
1363 INTIMATE group. Journal of Quaternary Science, 13, (4), 283-292.

1364 Bleil, U. & Dobeneck, Von, T., 1999. Geomagnetic events and relative paleointensity
1365 records—Clues to high-resolution paleomagnetic chronostratigraphies of Late
1366 Quaternary marine sediments? *Use of proxies in paleoceanography,* pp. 635-
1367 654.

1368 Broecker, W.S., 1998. Paleocean circulation during the last deglaciation: a bipolar
1369 seesaw? *Paleoceanography*, 13 (2), pp. 119-121.

1370 Bronk Ramsey, C., Scott, E. M. and van der Plicht, J., 2013. Calibration for
1371 Archaeological and Environmental Terrestrial Samples in the Time Range 26–50
1372 ka cal BP. *Radiocarbon*, 55 (4), pp. 2021–2027.

1373 Bronk Ramsey, C., 2008. Deposition models for chronological records. *Quaternary*
1374 *Science Reviews*, 27 (1-2), pp. 42–60.

1375 Bronk Ramsey, C., 2013. OxCal 4.2. Manual [online] available at:
1376 https://c14.arch.ox.ac.uk/oxcal.

1377 Carey, S., 1997. Influence of convective sedimentation on the formation of

1378 widespread tephra fall layers in the deep sea. *Geology*, 25 (9), pp. 839–842.

1379 Chamberlain, K. J., Morgan, D. J. and Wilson, C., 2014. Timescales of mixing and
1380 mobilisation in the Bishop Tuff magma body: perspectives from diffusion
1381 chronometry. *Contributions to Mineralogy and Petrology,* 168:1034.

1382 Channell, J. E. T., Xuan, C. and Hodell, D. A., 2009. Stacking paleointensity and
1383 oxygen isotope data for the last 1.5 Myr (PISO-1500). *Earth and Planetary*
1384 *Science Letters*, 283 (1-4), pp. 14-23.

1385 Channell, J.E.T., Hodell, D. A., Singer, B. S. and Xuan, C., 2010. Reconciling
1386 astrochronological and $^{40}Ar/^{39}Ar$ ages for the Matuyama□Brunhes boundary and
1387 late Matuyama Chron. *Geochemistry, Geophysics, Geosystems*, 11 (12).

1388 Chen, C.H. Lee, M. Y., Lizuka, Y., Dehn, J., Wei, K. Y. and Carey, S., 2004. First
1389 Toba supereruption revival: Comment and Reply REPLY. *Geology,* 32 (1), pp.
1390 54-55.

1391 Chen, J., Farrell, J. W., Murray, D. W., Warren, L. P., 1995. Timescale and
1392 paleoceanographic implications of a 3.6 my oxygen isotope record from the
1393 northeast Indian Ocean (Ocean Drilling Program site 758). *Paleoceanography*,
1394 10 (1), pp. 21-47.

1395 Chesner, C.A. & Rose, W.I., 1991. Stratigraphy of the Toba tuffs and the evolution of
1396 the Toba caldera complex, Sumatra, Indonesia. *Bulletin of Volcanology*. 53, pp.
1397 343-356.

1398 Chesner, C.A., Rose, W. I., Deino, A., Drake, R. and Westgate, J. A., 1991. Eruptive
1399 history of Earth's largest Quaternary caldera (Toba, Indonesia) clarified.
1400 *Geology.* 19 (3), pp. 200-203.

1401 Christiansen, R. L., 2001. The Quaternary and Pliocene Yellowstone Plateau

1402 volcanic field of Wyoming, Idaho, and Montana. *US Geological Survey*
1403 *Professional Paper*, (729 G), pp.G1–G145.

1404 Clement, B.M., 2004. Dependence of the duration of geomagnetic polarity reversals
1405 on site latitude. *Nature*, 428 (6983), pp.637–640.

1406 Coe, R.S., Singer, B. S., Pringle, M. S. and Zhao, X., 2004. Matuyama–Brunhes
1407 reversal and Kamikatsura event on Maui: paleomagnetic directions, $^{40}Ar/^{39}Ar$
1408 ages and implications. *Earth and Planetary Science Letters.* 222 (2), pp. 667-
1409 684.

1410 Crowley, J. L., Schoene, B. & Bowring, S. A., 2007. U-Pb dating of zircon in the
1411 Bishop Tuff at the millennial scale. *Geology*, 35 (12), pp.1123–1126.

1412 Dehn, J., Farrell, J. W. and Schmincke, H. U., 1991. Neogene tephrochronology from
1413 Site 758 on northern Ninetyeast Ridge: Indonesian arc volcanism of the past 5
1414 Ma. *Proceedings of the Ocean Drilling Program, scientific results.* 121, pp. 273-
1415 295.

1416 Diehl, J., 1987. No short reversals of Brunhes age recorded in the Toba tuffs, North
1417 Sumatra, Indonesia. *Geophysical Research Letters*, 14 (7), pp.753–756.

1418 Duplessy, J. C., Bard, E., Arnold, M., Shackleton, N. J., Duprat, J. and Labeyrie, L.,
1419 1991. How Fast Did the Ocean - Atmosphere System Run During the Last
1420 Deglaciation? *Earth and Planetary Science Letters*, 103 (1-4), pp. 27–40.

1421 Farrell, J.W. & Janecek, T.R., 1991. Late Neogene paleoceanography and
1422 paleoclimatology of the northeast Indian Ocean (Site 758). *In proceedings,*
1423 *Ocean Drilling Program, Scientific Results.* 121: College Station, Texas, Ocean
1424 Drilling Program, pp. 297-355.

1425 Gee, J., Tauxe, L. and Barg, E., 1991. *17.* Lower Jaramillo polarity transition records

1426 from the equatorial Atlantic and Indian oceans. *In proceedings, Ocean Drilling*
1427 *Program, scientific results,* 121, pp. 377-391.

1428 Giaccio, B., Regattieri, E., Zanchetta, G., Wagner, B., Galli, P., Manella, G.,
1429 Niespolo, E., Peronace, E., Renne, P.R., Nomade, S., Cavinato, G.P., Messina,
1430 P., Sposato, A., Boschi, C., Florindo, F., Marra, F. & Sadori, L., 2015. A key
1431 continental archive for the last 2 Ma of climatic history of the central
1432 mediterranean region: A pilot drilling in the Fucino Basin, central Italy. Scientific
1433 Drilling, 20, 13-19.

1434 Glass, B.P. & Koeberl, C., 2006. Australasian microtektites and associated impact
1435 ejecta in the South China Sea and the Middle Pleistocene supereruption of Toba.
1436 Meteoritics & Planetary Science, 41, 305-326.

1437 Hall, C.M. & Farrell, J.W., 1995. Laser 40Ar/39Ar ages of tephra from Indian Ocean
1438 deep-sea sediments: Tie points for the astronomical and geomagnetic polarity
1439 time scales. Earth and Planetary Science Letters, 133, 93-4), 327-328.

1440 Hartl, P. and Tauxe, L., 1996. A precursor to the Matuyama/Brunhes transition-field
1441 instability as recorded in pelagic sediments. *Earth and Planetary Science Letters*,
1442 138 (1-4), pp. 121-135.

1443 Hays, J.D., Imbrie, J. and Shackleton, N.J., 1976. Variations in the Earth's orbit:
1444 pacemaker of the ice ages. *Science,* 194 (4270), pp. 1121-1132.

1445 Horng, C.S., Lee, M. Y., Pälike, H., Wei, K. Y., Liang, W. T., Iizuka, Y. and Torii, M.,
1446 2002. Astronomically calibrated ages for geomagnetic reversals within the
1447 Matuyama chron. *Earth Planets Space,* 54, pp. 679-690.

1448 Hyodo, M., Matsu'ura, S., Kamishima, Y., Kondo, M., Takeshita, Y., Kitaba, I.,
1449 Danhara, T., Aziz, F., Kurniawan, I. and Kumai, H., 2011. High-resolution record

of the Matuyama-Brunhes transition constrains the age of Javanese Homo erectus in the Sangiran dome, Indonesia. *Proceedings of the National Academy of Sciences of the United States of America*, 108 (49), pp.19563–19568.

Ickert, R. B., Mundil, R., Magee Jr., C. W. and Mulcahy, S. R., 2015. The U–Th–Pb systematics of zircon from the Bishop Tuff: A case study in challenges to high-precision Pb/U geochronology at the millennial scale. *Geochemica et Cosmochimica Acta*, 168, pp. 88-110.

Imbrie, J. and Imbrie, J. Z., 1980. Modeling the climatic response to orbital variations. *Science,* 207 (4434), pp. 943-953.

Imbrie, J., Hays, J. D., Martinson, D. G., McIntyre, A., Mix, A. C., Morley, J. J., Pisias, N. G., Prell, W. L. and Shackleton, N. J., 1984. The orbital theory of Pleistocene climate: support from a revised chronology of the marine $\delta^{18}O$ record. *Milankovitch and climate: Understanding the response to astronomical forcing, proceedings of the NATO advanced research workshop held 30 November - 4 December, 1982 in Palisades, N.Y. Edited by A. Berger, J. Imbrie, H. Hays, G. Kukla and B. Saltzman.* pp. 269.

Jarosewich, E., Nelen, J. A. and Norberg, J. A., 1980. Reference Samples for Electron Microprobe Analysis*. *Geostandards newsletter,* 4 (1), pp. 43-47.

Jin, C. and Liu, Q., 2011. Remagnetization mechanism and a new age model for L9 in Chinese loess. *Physics of the Earth and Planetary Interiors*, 187 (3-4), pp.261–275.

Jochum, K. P., Stoll, B. and Herwig, K., *et al.,* 2006. MPI□DING reference glasses for in situ microanalysis: New reference values for element concentrations and isotope ratios. *Geochemistry*, *Geophysics, Geosystems.* 7 (2).

1474 Johnson, R. G., 1982. Brunhes-Matuyama magnetic reversal dated at 790,000 yr BP
1475 by marine-astronomical correlations. *Quaternary Research*. 17 (2), pp. 135-147.

1476 Katsuta, N., Takano, M., Kawakami, S. I., Togami, S., Fukusawa, H., Kumazawa, M.
1477 and Yasuda, Y., 2007. Advanced micro-XRF method to separate sedimentary
1478 rhythms and event layers in sediments: its application to lacustrine sediment
1479 from Lake Suigetsu, Japan. *Journal of Paleolimnology.* 37 (2), pp. 259-271.

1480 Kent, D. V., 1973. Paleomagnetism of some Neogene sedimentary rocks on Oga
1481 Peninsula, Japan. *Journal of geomagnetism and geoelectricity*. 25, pp. 87-103.

1482 Kent, D. V. and Schneider, D. A., 1995. Correlation of paleointensity variation
1483 records in the Brunhes/Matuyama polarity transition interval. *Earth and Planetary*
1484 *Science Letters*, 129 (1-4), pp. 135–144.

1485 Kissel, C., Guillo, H., Laj, C., Carracedo, J.C., Perez-Torrado, F., Wandres, C., et al.,
1486 2014. A combined paleomagnetic/dating investigation of the upper Jaramillo
1487 transition from a volcanic section at Tenerife (Canary Islands). Earth Planetary
1488 Science Letters, 406, 59-71.

1489 Knight, M. D., Walker, G., Ellwood, B. B. and Diehl, J. F., 1986. Stratigraphy,
1490 paleomagnetism, and magnetic fabric of the Toba Tuffs: constraints on the
1491 sources and eruptive styles. *Journal of Geophysical Research.* 91, pp. 355-382.

1492 Kuiper, K. F., Deino, A., Hilgen, F. J., Krijgsman, W., Renne, P. R. and Wijbrans, J.
1493 R., 2008. Synchronizing Rock Clocks of Earth History. *Science*, 320 (5875),
1494 pp.500–504.

1495 Labeyrie, L., Waelbroeck, C., Cortijo, E., Michel, E. and Duplessy, J. C., 2005.
1496 Changes in deep water hydrology during the Last Deglaciation. *Comptes Rendus*
1497 *Geoscience.* 337 (10-11), pp. 919-927.

1498 Langereis, C. G., Dekkers, M. J., de Lange, G. J., Paterne, M. and van Santvoort, P.
1499 J. M., 1997. Magnetostratigraphy and astronomical calibration of the last 1.1 Myr
1500 from an eastern Mediterranean piston core and dating of short events in the
1501 Brunhes. *Geophysical Journal International*, 129 (1), pp.75–94.

1502 Lanphere, M. A. and Baadsgaard, H., 2001. Precise K–Ar, $^{40}Ar/^{39}Ar$, Rb–Sr and U/Pb
1503 mineral ages from the 27.5 Ma Fish Canyon Tuff reference standard. *Chemical*
1504 *Geology*, 175 (3-4), pp. 653–671.

1505 Laskar, J., Robutel, P., Joutel, F., Gastineau, M., Correia, A. C. M. and Levrard, B.,
1506 2004. A long-term numerical solution for the insolation quantities of the Earth.
1507 *Astronomy and Astrophysics*, 428 (1), pp. 261–285.

1508 Laskar, J., Joutel, F. and Robutel, P., 1993. Stabilization of the Earth's obliquity by
1509 the Moon. *Nature*, 361 (6413), pp. 615–617.

1510 Lee, J. Y., Marti, K., Severinghaus, J. P., Kawamura, K., Yoo, H. S., Lee, J. B. and
1511 Kim, J. S., 2006. A redetermination of the isotopic abundances of atmospheric
1512 Ar. *Geochimica et Cosmochimica Acta*, 70 (17), pp. 4507-4512.

1513 Lee, M.Y., Chen, C. H., Wei, K. Y., Iizuka, Y. and Carey, S., 2004. First Toba
1514 supereruption revival. *Geology*, 32 (1), pp. 61-64.

1515 Leonhardt, R. & Fabian, K., 2007. Paleomagnetic reconstruction of the global
1516 geomagnetic field evolution during the Matuyama/Brunhes transition: Iterative
1517 Bayesian inversion and independent verification. *Earth and Planetary Science*
1518 *Letters*, 253 (1-2), pp. 172-195.

1519 Lisiecki, L. E. & Raymo, M. E., 2005. A Pliocene□Pleistocene stack of 57 globally
1520 distributed benthic $\delta^{18}O$ records. *Paleoceanography*, 20 (1).

1521 Lisiecki, L. E. & Raymo, M. E., 2009. Diachronous benthic $\delta^{18}O$ responses during

late Pleistocene terminations. *Paleoceanography*, 24 (3).

Liu, Q., Roberts, A. P., Rohling, E. J., Zhu, R. and Sun, Y., 2008. Post-depositional remanent magnetization lock-in and the location of the Matuyama–Brunhes geomagnetic reversal boundary in marine and Chinese loess sequences. *Earth and Planetary Science Letters*, 275 (1-2), pp. 102–110.

Macken, A. C., Staff, R. A. and Reed, E. H., 2013. Bayesian age-depth modelling of Late Quaternary deposits from Wet and Blanche Caves, Naracoorte, South Australia: A framework for comparative faunal analyses. *Quaternary Geochronology*, 17, pp. 26–43.

Mark, D. F., Petraglia, M., Smith, V. C., Morgan, L. E., Barfod, D. N., Ellis, B. S., Pearce, N. J., Pal, J. N. and Korisettar, R., 2014. A high-precision $^{40}Ar/^{39}Ar$ age for the Young Toba Tuff and dating of ultra-distal tephra: Forcing of Quaternary climate and implications for hominin occupation of India. *Quaternary Geochronology*, 21, pp. 90–103.

Mark, D. F., Petraglia, M., Smith, V. C., Morgan, L. E., Barfod, D. N., Ellis, B. S., Pearce, N. J., Pal, J. N. and Korisettar, R., 2013. Multiple interpretive errors? Indeed. Reply to: Climate effects of the 74ka Toba super-eruption: Multiple interpretive errors in 'A high-precision $^{40}Ar/^{39}Ar$ age for the Young Toba Tuff and dating of ultra-distal tephra' by Michael Haslam. *Quaternary Geochronology,* 18, pp. 173-175.

Mark, D. F., Gonzalez, S., Huddart, D. and Böhnel, H., 2010. Dating of the Valsequillo volcanic deposits: Resolution of an ongoing archaeological controversy in Central Mexico. *Journal of human evolution*, 58 (5), pp. 441-445.

Mark, D. F., Stuart, F. M. and de Podesta, M., 2011. New high-precision measurements of the isotopic composition of atmospheric argon. *Geochimica et*

1547 *Cosmochimica Acta*, 75 (23), pp. 7494–7501.

1548 Martinson, D.G., Pisias, N., Hays, D.J., Imbrie, J., Moore, T.C. & Shackleton, N.J.,
1549 1987. Age dating and the orbital theory of the ice ages: development of a high-
1550 resolution 0 to 300,000-year chronostatigraphy. Quaternary Research, 27, 1-30.

1551 Matthews, N. E., Vazquez, J. A. and Calvert, A. T., 2015. Age of the Lava Creek
1552 supereruption and magma chamber assembly at Yellowstone based on $^{40}Ar/^{39}Ar$
1553 and U-Pb dating of sanidine and zircon crystals. *Geochemistry, Geophysics,*
1554 *Geosystems*, 16 (8), pp. 2508–2528.

1555 McDougall, I. and Harrison, T. M., 1999. Geochronology and Thermochronology by
1556 the $^{40}Ar/^{39}Ar$ Method. *Oxford University Press, New York.*

1557 Milankovitch, M., 1930. Mathematische Klimalehre und Astronomische Theorie der
1558 Klimaschwankungen, Handbuch der Klimalogie Band 1 Teil A Borntrager Berlin.

1559 Min, K., Mundil, R., Renne, P. R. and Ludwig, K. R., 2000. A test for systematic
1560 errors in $^{40}Ar/^{39}Ar$ geochronology through comparison with U/Pb analysis of a
1561 1.1-Ga rhyolite. *Geochimica et Cosmochimica Acta*, 64 (1), pp. 73–98.

1562 Morgan, L. E., Mark, D. F., Imlach, J., Barfod, D. and Dymock, R., 2014. FCs-EK: a
1563 new sampling of the Fish Canyon Tuff $^{40}Ar/^{39}Ar$ neutron flux monitor. *Geological*
1564 *Society, London, Special Publications*, 378 (1), pp. 63–67.

1565 Niespolo, E.M., Rutte, D., Deino, A.L. & Renne, P.R., 2016. Intercalibration and age
1566 of the Alder Creek sanidine 40Ar/39Ar standard. Quaternary Geochronology.

1567 Nomade, S., Renne, P. R., Vogel, N., Deino, A. L., Sharp, W. D., Becker, T. A.,
1568 Jaouni, A. R. and Mundil, R., 2005. Alder Creek sanidine (ACs-2): A Quaternary
1569 $^{40}Ar/^{39}Ar$ dating standard tied to the Cobb Mountain geomagnetic event.
1570 *Chemical Geology,* 218 (3-4), pp. 315-338.

1571 Olson, P., 2011. Laboratory Experiments on the Dynamics of the Core. *Physics of*
1572 *the Earth and Planetary Interiors*, 187 (1), pp. 1-18.

1573 Parrenin, F. and Paillard, D., 2003. Amplitude and phase of glacial cycles from a
1574 conceptual model. *Earth and Planetary Science Letters*, 214 (1-2), pp. 243–250.

1575 Parrenin, F., Barnola, J. M., Beer, J. et al., 2007. The EDC3 chronology for the
1576 EPICA Dome C ice core. *Climate of the Past,* 3, pp. 485-497.

1577 Peirce, J., 1989. Proceedings, initial reports, Ocean Drilling Program, Leg 121,
1578 Broken Ridge and Ninetyeast Ridge. Volume 121.

1579 Raisbeck, G., Yiou, F., Jouzel, J. and Stocker, T. F., 2007. Direct north-south
1580 synchronization of abrupt climate change record in ice cores using Beryllium 10.
1581 *Climate of the Past,* 3, pp. 541-547.

1582 Reid, M. R. and Coath, C. D., 2000. In situ U-Pb ages of zircons from the Bishop
1583 Tuff: No evidence for long crystal residence times. *Geology*, 28, 443-446.

1584 Renne, P.R., 2014. Some footnotes to the optimization-based calibration of the
1585 $^{40}Ar/^{39}Ar$ system. *Geological Society, London, special publications,* 378, pp. 21-
1586 31.

1587 Renne, P. R. and Norman, E. B., 2001. Determination of the half-life of ^{37}Ar by mass
1588 spectrometry. *Physical Review C*, 63 (4), 047302.

1589 Renne, P. R., Swisher, C. C., Deino, A. L., Karner, D. B., Owens, T. L. and DePaolo,
1590 D. J., 1998. Intercalibration of standards, absolute ages and uncertainties in
1591 $^{40}Ar/^{39}Ar$ dating. *Chemical Geology,* 145 (1-2), pp. 117-152.

1592 Renne, P. R., Mundil, R., Balco, G., Min, K. and Ludwig, K. R., 2010. Joint
1593 determination of ^{40}K decay constants and $^{40}Ar^{*}/^{40}K$ for the Fish Canyon sanidine

1594 standard, and improved accuracy for $^{40}Ar/^{39}Ar$ geochronology. *Geochimica et*
1595 *Cosmochimica Acta*, 74 (18), pp. 5349–5367.

1596 Renne, P.R., Mundil, R., Balco, G., Min, K. and Ludwig, K. R., 2011. Response to the
1597 comment by W. H. Schwarz et al. on "Joint determination of ^{40}K decay constants
1598 and $^{40}Ar^{*}/^{40}K$ for the Fish Canyon sanidine standard, and improved accuracy for
1599 $^{40}Ar/^{39}Ar$ geochronology. *Geochimica et Cosmochimica Acta,* 75, pp. 5097-5100.

1600 Renne, P. R., Deino, A. L., Hilgen, F. J., Kuiper, K. F., Mark, D. F., Mitchell III, W. S.,
1601 Morgan, L. E., Mundil, R. and Smit, J., 2013. Time Scales of Critical Events
1602 Around the Cretaceous-Paleogene Boundary. *Science*, 339 (6120), pp. 684–687.

1603 Renne, P.R., Cassata, W.S. & Morgan, L.E., 2009. The isotopic composition of
1604 atmospheric argon and $^{40}Ar/^{39}Ar$ geochronology: Time for a change? *Quaternary*
1605 *Geochronology*, 4 (4), pp. 288-298.

1606 Renne, P. R., Sharp, Z. D. and Heizler, M. T., 2008. Cl-derived argon isotope
1607 production in the CLICIT facility of OSTR reactor and the effects of the Cl-
1608 correction in $^{40}Ar/^{39}Ar$ geochronology. *Chemical Geology*, 255 (3-4), pp. 463-466.

1609 Rivera, T. A., Storey, M., Zeeden, C., Hilgen, F. J. and Kuiper, K., 2011. A refined
1610 astronomically calibrated $^{40}Ar/^{39}Ar$ age for Fish Canyon sanidine. *Earth and*
1611 *Planetary Science Letters*, 311 (3-4), pp. 420–426.

1612 Rivera, T. A., Storey, M., Schmitz, M. D. and Crowley, J. L., 2013. Age
1613 intercalibration of $^{40}Ar/^{39}Ar$ sanidine and chemically distinct U/Pb zircon
1614 populations from the Alder Creek Rhyolite Quaternary geochronology standard.
1615 *Chemical Geology*, 345, pp. 87–98.

1616 Roberts, A. P. and Winklhofer, M., 2004. Why are geomagnetic excursions not
1617 always recorded in sediments? Constraints from post-depositional remanent

1618 magnetization lock-in modelling. *Earth and Planetary Science Letters*, 227 (3-4),
1619 pp. 345-359.

1620 Ruddiman, W. F., Raymo, M. E., Martinson, D.G., Clement, B. M. and Backman, J.,
1621 1989. Pleistocene evolution: northern hemisphere ice sheets and North Atlantic
1622 Ocean. *Paleoceanography,* 4 (4), pp. 353-412.

1623 Sagnotti, L., Giaccio, B. and Liddicoat, J. C. et al., 2016. How fast was the
1624 Matuyama–Brunhes geomagnetic reversal? A new subcentennial record from the
1625 Sulmona Basin, central Italy. *Geophysical Journal International,* 204 (2), pp. 798-
1626 812.

1627 Sagnotti, L., Scardia, G. and Giaccio, B. et al., 2014. Extremely rapid directional
1628 change during Matuyama-Brunhes geomagnetic polarity reversal. *Geophysical*
1629 *Journal International,* 199 (2), pp. 1110-1124.

1630 Schlolaut, G., Marshall, M. H. and Brauer, A. et al., 2012. An automated method for
1631 varve interpolation and its application to the Late Glacial chronology from Lake
1632 Suigetsu, Japan. *Quaternary Geochronology*, 13, pp. 52–69.

1633 Shackleton, N. J., Berger, A. & Peltier, W. R., 1990. An alternative astronomical
1634 calibration of the lower Pleistocene timescale based on ODP Site 677.
1635 *Transactions of the Royal Society of Edinburgh: Earth Sciences*, 81 (04), pp.
1636 251–261.

1637 Shane, P., Westgate, J., Williams, M. and Korisettar, R., 1995. New Geochemical
1638 Evidence for the Youngest Toba-Tuff in India. *Quaternary Research*, 44 (2), pp.
1639 200–204.

1640 Shane, P., Self, S., Blake, S. & Rampino, M.R., 2004. First Toba supereruption
1641 revival: Comment and Reply. Geology, 32, (1), 54.

1642 Shipboard Scientific Party, 1989. doi:10.2973/odp.proc.ir.121.112.1989.

1643 Shulmeister, J., Rodbell, D. T., Gagan, M. K. and Seltzer, G. O., 2006. Inter-
1644 hemispheric linkages in climate change: paleo-perspectives for future climate
1645 change. *Climate of the Past*, 2 (2), pp. 167–185.

1646 Simon, J. I. and Reid, M. R., 2005. The pace of rhyolite differentiation and storage in
1647 an "archetypical" silicic magma system, Long Valley, California. *Earth and*
1648 *Planetary Science Letters*, 235 (1-2), pp. 123–140.

1649 Simon, J. I., Weis, D., DePaolo, D. J. and Renne, P. R. et al., 2014. Assimilation of
1650 preexisting Pleistocene intrusions at Long Valley by periodic magma recharge
1651 accelerates rhyolite generation: rethinking the remelting model. *Contributions to*
1652 *Mineralogy and Petrology*, 167:955.

1653 Simon, J. I., Renne, P. R. and Mundil, R., 2008. Implications of pre-eruptive
1654 magmatic histories of zircons for U-Pb geochronology of silicic extrusions. *Earth*
1655 *and Planetary Science Letters*, 266 (1-2), pp. 182–194.

1656 Singer, B. S., 2014. A Quaternary geomagnetic instability time scale. *Quaternary*
1657 *Geochronology*, 21, pp. 29-52.

1658 Singer, B. S. and Pringle, M. S., 1996. Age and duration of the Matuyama-Brunhes
1659 geomagnetic polarity reversal from $^{40}Ar^{39}Ar$ incremental heating analyses of
1660 lavas. *Earth and Planetary Science Letters*, 139 (1-2), pp. 47-61.

1661 Singer, B. S., Hoffman, K. A. and Coe, R. S. et al., 2005. Structural and temporal
1662 requirements for geomagnetic field reversal deduced from lava flows. *Nature*,
1663 434, pp. 633-636.

1664 Skinner, L. C. and Shackleton, N. J., 2005. An Atlantic lead over Pacific deep-water
1665 change across Termination I: implications for the application of the marine

1666 isotope stage stratigraphy. *Quaternary Science Reviews*, 24 (5-6), pp. 571–580.

1667 Smit, J., van Eijden, A. and Troelstra, S. R., 1991. Analysis of the Australasian
1668 microtektite event, the Toba Lake event, and the Cretaceous/Paleogene
1669 boundary, Eastern Indian Ocean. *In proceedings, Ocean Drilling Program,*
1670 *scientific results,* 121, pp. 489-503.

1671 Smith, V.C., Staff, R.A., Blockley, S.P.E., Bronk Ramsey, C., Nakagawa, T., Mark,
1672 D.F., Takemura, K., Danhara, T., 2013, Identification and correlation of visible
1673 tephras in the Lake Suigetsu SG06 sedimentary archive, Japan:
1674 chronostratigraphic markers for synchronising of east Asian/west Pacific
1675 palaeoclimatic records across the last 150 ka. *Quaternary Science Reviews*, 67,
1676 pp. 121–137.

1677 Smith, V.C., Mark, D.F., Staff, R.A., Blockley, S.P.E., Bronk Ramsey, C., Bryant,
1678 C.L., Nakagawa, T., Han, K.K., Weh, A., Takemura, K., Danhara, T. & Suigetsu
1679 2006 Project Members, 2011. Toward establishing precise $^{40}Ar/^{39}Ar$ chronologies
1680 for Late Pleistocene palaeoclimate archives: an example from the Lake Suigetsu
1681 (Japan) sedimentary record. *Quaternary Science Reviews*, 30(21-22), pp. 2845–
1682 2850.

1683 Staff, R.A., Nakagawa, T., Schlolaut, G., Marshall, M.H., Brauer, A., Lamb, H.F.,
1684 Bronk Ramsey, C., Bryant, C.L., Brock, F., Kitagawa, H., van der Plicht, J.,
1685 Payne, R.L., Smith, V.C., Mark, D.F., Macleod, A., Blockley, S.P.E.,
1686 Schwenninger, J.L., Tarasov, P.E., Haraguchi, T., Gotanda, K., Yonenobu, H.,
1687 Yokoyama, Y. & Suigetsu 2006 Project Members, 2013. The multiple
1688 chronological techniques applied to the Lake Suigetsu SG06 sediment core,
1689 central Japan. *Boreas*, 42(2), pp. 259–266.

1690 Steiger, R.H. & Jager, E., 1977. *Subcommission on geochronology-convention on*

use of decay constants in geochronology and cosmochronology, Earth and Planetary Science Letters, 36, pp. 359-362.

Stoenner, R.W., Oa, S. & Katcoff, S., 1965. Half-Lives of Argon-37 Argon-39 and Argon-42. *Science*, 148(3675), pp. 1325.

Stocker, T.F., & Johnsen, S.J., 2003. A minimum thermodynamic model for the bipolar seesaw. Paleoceanography, 18, 1087.

Storey, M., Roberts, R. G. and Saidin, M., 2012. Astronomically calibrated Ar-40/Ar-39 age for the Toba supereruption and global synchronization of late Quaternary records. *Proceedings of the National Academy of Sciences of the United States of America*, 109 (46), pp. 18684–18688.

Suganuma, Y., Yokoyama, Y., Yamazaki, T., Kawamura, K., Horng, C-S. & Matsuzaki, H., 2010. ^{10}Be evidence for delayed acquisition of remanent magnetization in marine sediments: Implication for a new age for the Matuyama–Brunhes boundary. *Earth and Planetary Science Letters*, 296(3-4), pp. 443–450.

Suganuma, Y., Okada, M., Horie, K., Kaiden, H., Takehara, M., Senda, R., Kimura J-I., Kawamura, K., Haneda, Y., Kazaoka, O. & Head, M.J., 2015. Age of Matuyama-Brunhes boundary constrained by U-Pb zircon dating of a widespread tephra. *Geology*, 43(6), pp. 491–494.

Suganuma, Y., Okuno, J., Heslop, D., Roberts, A.P., Yamazaki, T. & Yokoyama, Y., 2011. Post-depositional remanent magnetization lock-in for marine sediments deduced from ^{10}Be and paleomagnetic records through the Matuyama–Brunhes boundary. *Earth and Planetary Science Letters*, 311(1-2), pp.39–52.

Tauxe, L., Herbert, T., Shackleton, N.J. & York, Y.S., 1996. Astronomical calibration of the Matuyama-Brunhes boundary: Consequences for magnetic remanence

1715 acquisition in marine carbonates and the Asian loess sequences. *Earth and*
1716 *Planetary Science Letters*, 140(1-4), pp. 133–146.

1717 Waelbroeck, C., Levi, C., Duplessy, J.C., Labeyrie, L., Michel, E., Cortijo, E.,
1718 Bassinot, F. & Guichard, F., 2006. Distant origin of circulation changes in the
1719 Indian Ocean during the last deglaciation. *Earth and Planetary Science Letters*,
1720 243(1-2), pp. 244–251.

1721 Wang, X., Yang, Z., Lovlie, R., Sun, Z. & Pei, J., 2006. A magnetostratigraphic
1722 reassessment of correlation between Chinese loess and marine oxygen isotope
1723 records over the last 1.1Ma. *Physics of the Earth and Planetary Interiors*, 159(1-
1724 2), pp. 109–117.

1725 Wang, X., Lovlie, R., Chen, Y., Yang, Z. Pei, J. & Tang, L., 2014. The Matuyama–
1726 Brunhes polarity reversal in four Chinese loess records: high-fidelity recording of
1727 geomagnetic field behavior or a less than reliable chronostratigraphic marker?
1728 *Quaternary Science Reviews*, 101, pp. 61–76.

1729 Wojcicki, A.S., Pringle, M.S. & Wijbrans, J., 2000. New $^{40}Ar/^{39}Ar$ age of the Bishop
1730 Tuff from multiple sites and sediment rate calibration for the Matuyama□Brunhes
1731 boundary. *Journal of Geophysical Research,* 105, pp. 21431-21443.

1732 Wotzlaw, J-F., Bindeman, I.N., Stern, R.A., D'Abzac, F-X. & Schaltegger, U., 2015.
1733 Rapid heterogeneous assembly of multiple magma reservoirs prior to
1734 Yellowstone supereruptions. *Scientific Reports*, 5, pp. 1-10.

1735 Wotzlaw, J.F., Schaltegger, U., Frick, D.A., Dungan, M.A., Gerdes, A. & Gunther, D.,
1736 2013. Tracking the evolution of large-volume silicic magma reservoirs from
1737 assembly to supereruption. *Geology*, 41(8), pp. 867–870.

1738 Yamei, H., 2000. Mid-Pleistocene Acheulean-like Stone Technology of the Bose

1739 Basin, South China. *Science*, 287 (5458), pp. 1622–1626.

1740 Yang, S., Fang, X., Shi., Z., Lehmkuhl, F., Song, S., Han, Y. & Han, W., 2010. Timing
1741 and provenance of loess in the Sichuan Basin, southwestern China.
1742 *Palaeogeography, Palaeoclimatology, Palaeoecology*, 292(1-2), pp. 144–154.

1743 Zeeden, C., Rivera, T. A. and Storey, M., 2014. An astronomical age for the Bishop
1744 Tuff and concordance with radioisotopic dates. *Geophysical Research Letters*,
1745 41 (10), pp. 3478–3484.

1746 Zhou, W., Beck, J.W., Kong, X., An, Z., Qiang, X., Wu, Z., Xian, F. & Ao,H., 2014.
1747 Timing of the Brunhes-Matuyama magnetic polarity reversal in Chinese loess
1748 using 10Be. *Geology*, 42(6), pp. 467–470.

Table 1: Summary of $^{40}Ar/^{39}Ar$ ages and R-values for various samples

	ODP 758	Age (Ma)	±1s (analytical)	±1s (full)	R	± 1s
OTTA	Ash d	0.79238	0.0005	0.0006	0.66646	0.00042
OTTB	Ash D	0.78559	0.0007	0.0008	0.66075	0.00059
MTT	Ash C	0.50200	0.0006	0.0007	0.42219	0.00050
LCTB	N/A	0.62700	0.0015	0.0017	0.52734	0.00126
BT	N/A	0.76655	0.0004	0.0005	0.64473	0.00034

Age reclaculated from Storey et al., 2012; Mark et al., 2014 - Young Toba Tephra

Table 2: Constraints used in Bayesian modelling (depths provided as mbsl, see Figure 2 for composite scale)

	Core sampled	Thickness (cm)	Depth (mbsf)	Peak abundance depth (mbsf)	Reference	Geochem. Correlation (glass & biotite)
Ash A	ODP 758 1H	34	1.50-1.84		Dehn et al., 1991	YTT
Ash C	ODP 758 2H	23	7.12-7.35		Dehn et al., 1991	MTT
Ash D	ODP 758 2H	13	10.80-10.93		Dehn et al., 1991	OTTB (Haranggoal)
Ash d	ODP 758 2H	2	11.25-11.27		Dehn et al., 1991	OTTA (Siguragura)
Ash E	ODP 758 2H	5	11.62-11.67		Dehn et al., 1991	?
MBGR			10.75		Farrell & Janecek, 1991	
$JGE_{termination}$			14.2		Farrell & Janecek, 1991	
JGE_{onset}			15.28		Farrell & Janecek, 1991	
Australasian tektites		63	10.93-11.56	11.01	Lee et al., 2004	

Table 3: MBB extrapolation calculations from North American sections using LCTB-BT and BT-MBB

LCTB age (ka)	627.0 ± 1.5						
BT age (ka)	766.6 ± 0.4	Lake Tecopa	Great Salt Lake	Ventura	San joaquin	Fisher valley	
Stratigraphic distance from LCTB to BT	$\partial_{(s1)}$	8.0	9.7	253.0	12.0	21.2	m
Stratigraphic distance from BT to the MBB	$\partial_{(s2)}$	0.5	2.5	18.0	2.5	5.0	m
Time interval from LCTB to BT	$\partial_{(t1)}$	141600	141600	141600	141600	141600	years
Sedimentation rate	$SR = \partial_{(s1)}/\partial_{(t1)}$	0.000056	0.000069	0.001787	0.000085	0.000150	m/year
Time interval BT to MBB	$\partial_{(t2)} = \partial_{(s2)}/SR$	8850	36495	10074	29500	33396	years
MBB age	$BT_{age} + \partial_{(t2)}$	785250	812895	786474	805900	809796	years
MBB age	$BT_{age} + \partial_{(t2)})/1000$	774.5	801.7	775.7	794.8	798.7	ka
± (note 20% uncertainty assigned to all section measurements for extrapolation, ± propagated using linear uncertainty propagation)		1803	1803	1803	1803	1803	years
±		1.8	1.8	1.8	1.8	1.8	ka

Average ± St. Deviation MBB age (relative to the five different sections in N. America) = 776-802 ka

Mean ± SEM x SQRT(MSWD) MBB age (relative to the five different sections in N. America) = 789.1 ± 5.6 ka (68.2% confidence interval)

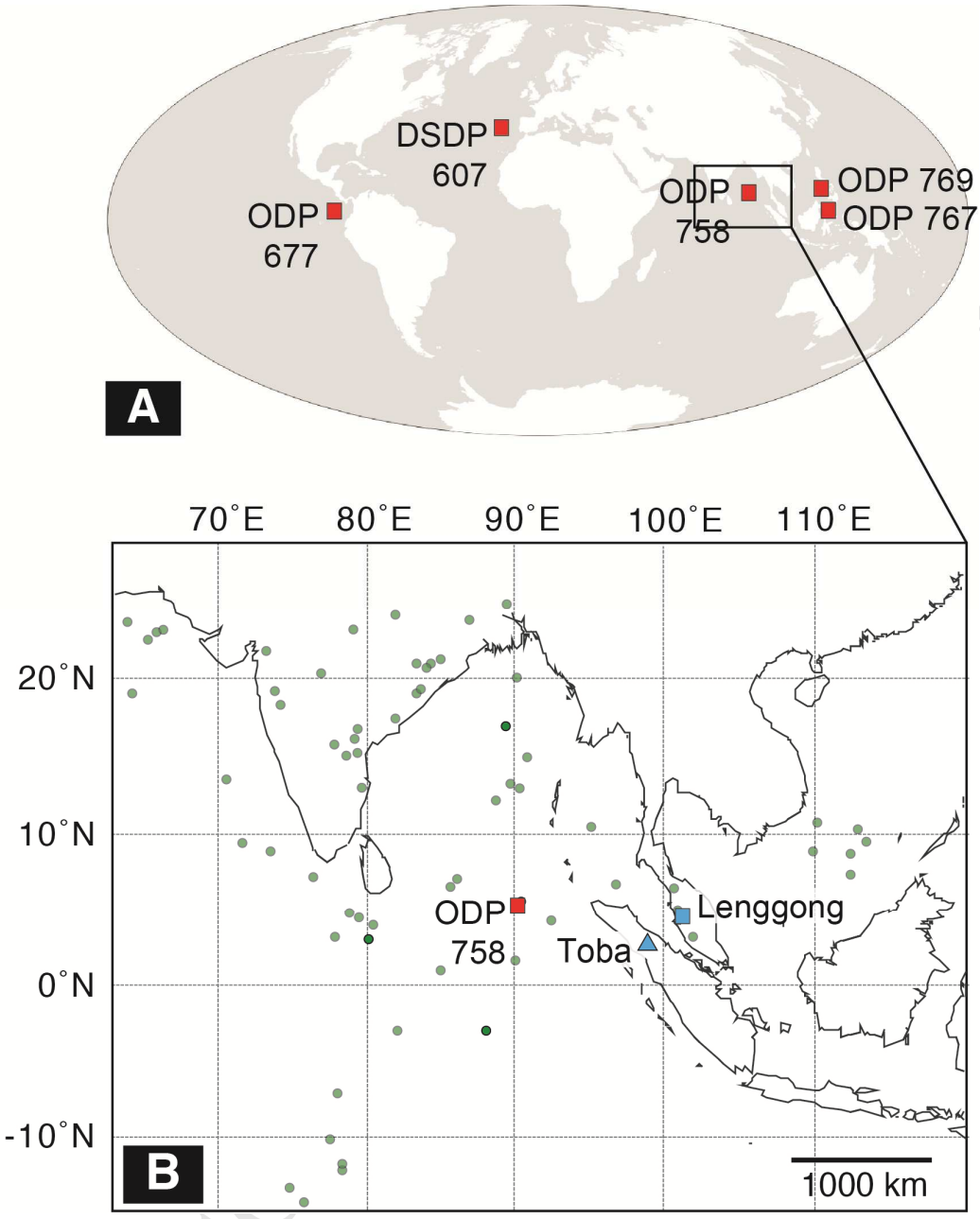
DSDP
607
ODP
677
ODP
758
ODP 769
ODP 767
A
70˚E
80˚E
90˚E
100˚E
110˚E
20˚N
10˚N
0˚N
-10˚N
ODP
758
Toba
Lenggong
B
1000 km

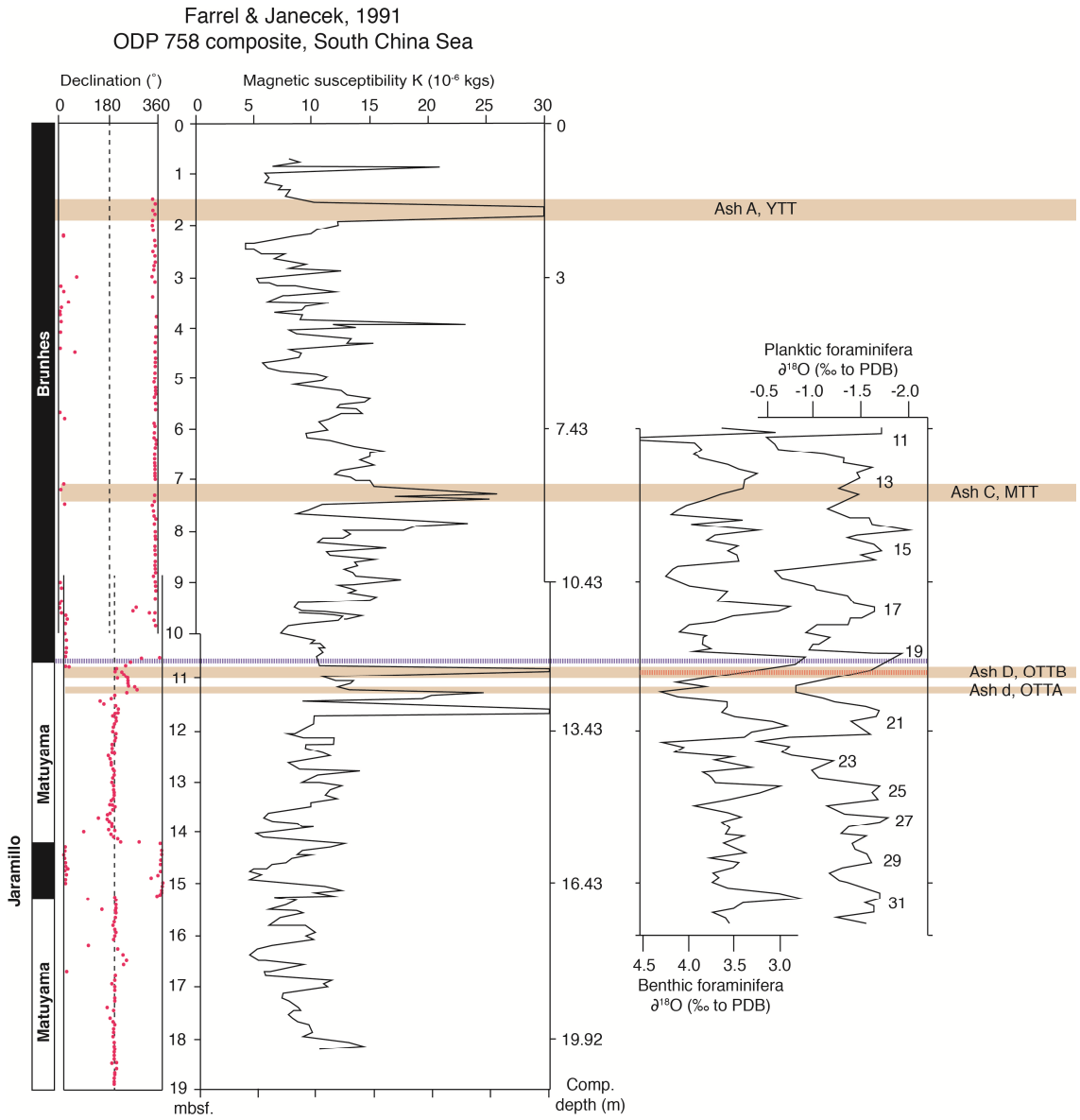

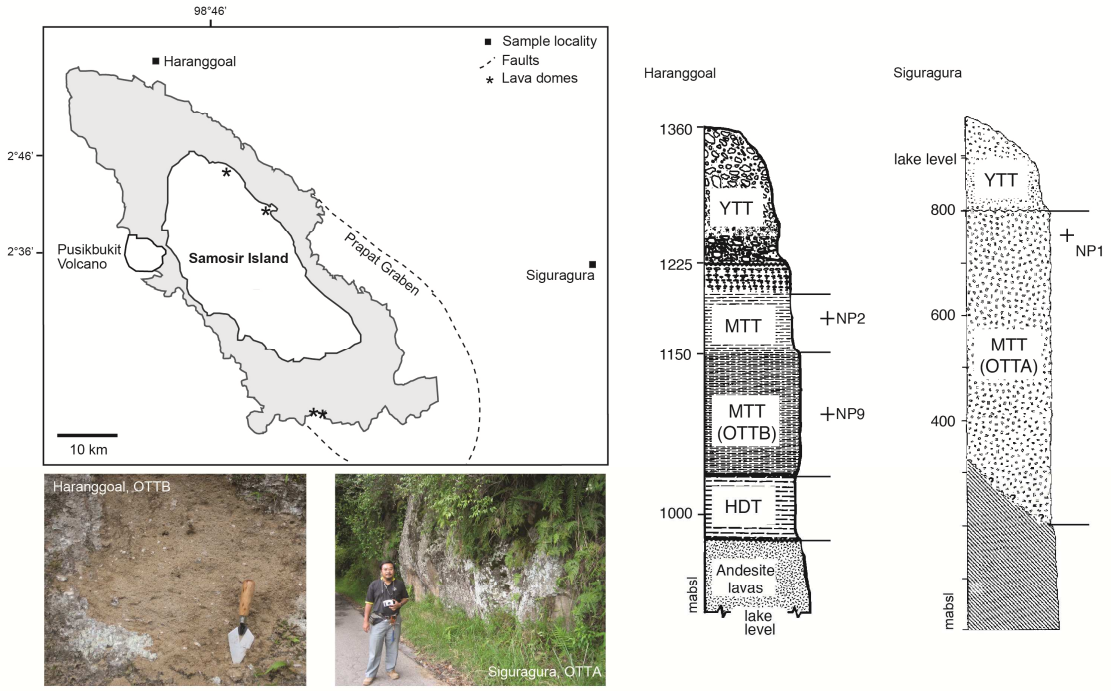

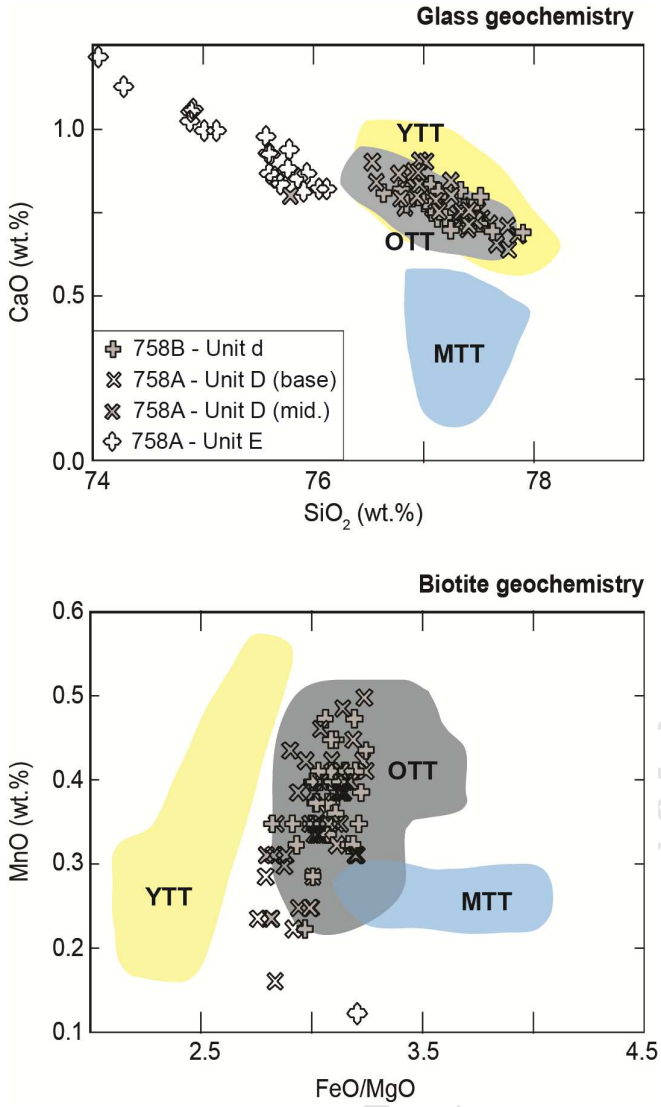

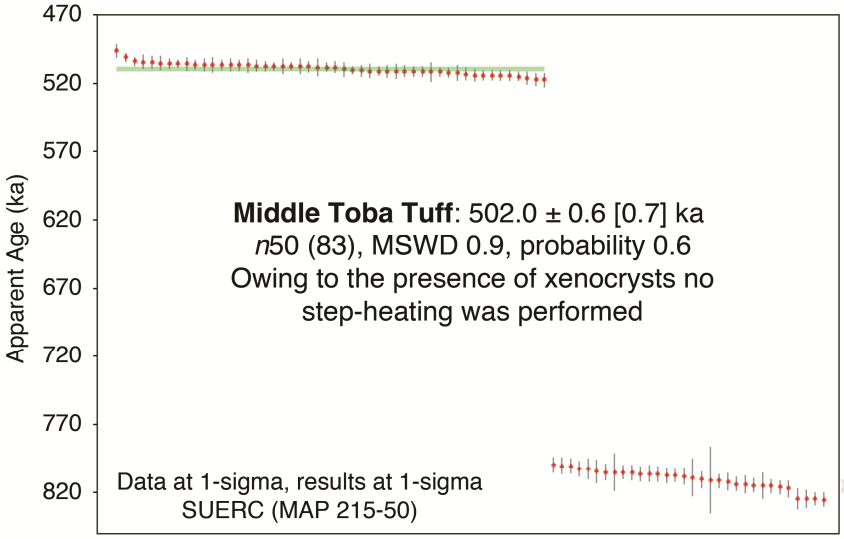
Apparent Age (ka)
470
520
570
620
670
720
770
820
Middle Toba Tuff: 502.0 ± 0.6 [0.7] ka
n50 (83), MSWD 0.9, probability 0.6
Owing to the presence of xenocrysts no
step-heating was performed
Data at 1-sigma, results at 1-sigma
SUERC (MAP 215-50)

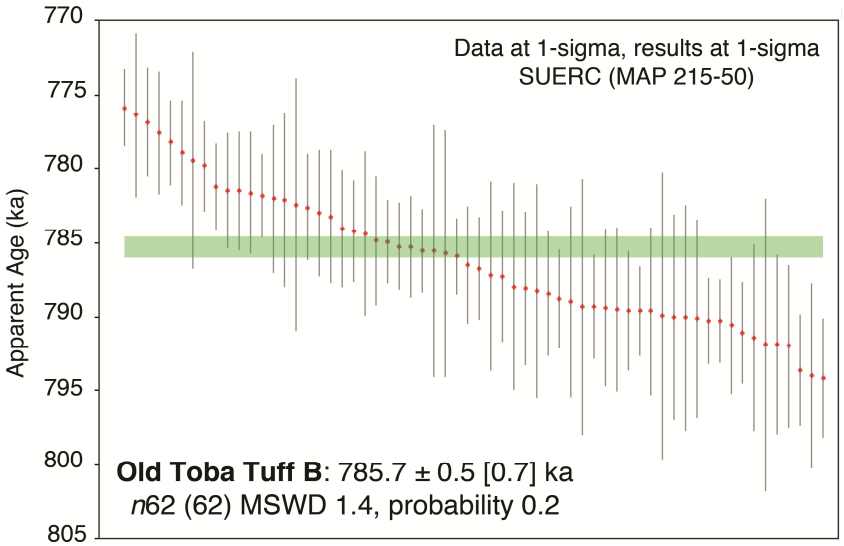
Apparent Age (ka)
770
775
780
785
790
795
800
805
Data at 1-sigma, results at 1-sigma
SUERC (MAP 215-50)
Old Toba Tuff B: 785.7 ± 0.5 [0.7] ka
n62 (62) MSWD 1.4, probability 0.2

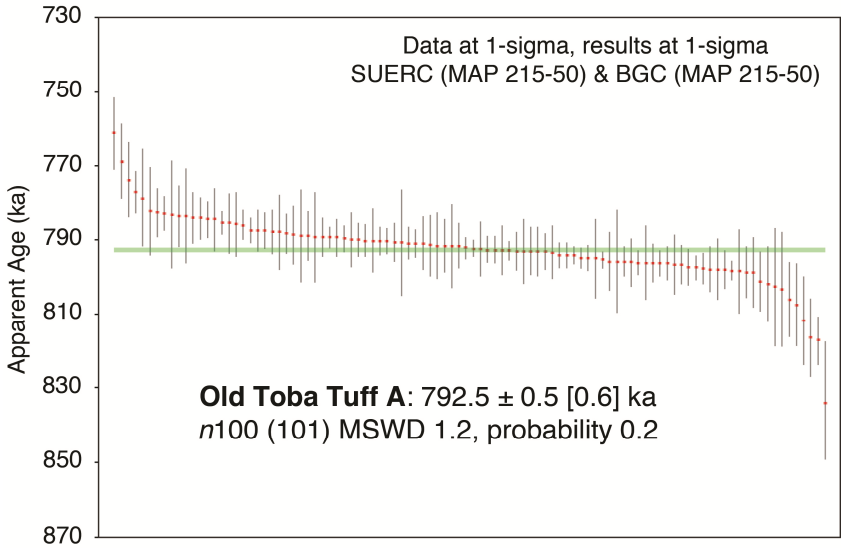
Apparent Age (ka)
730
750
770
790
810
830
850
870
Data at 1-sigma, results at 1-sigma
SUERC (MAP 215-50) & BGC (MAP 215-50)
Old Toba Tuff A: 792.5 ± 0.5 [0.6] ka
n100 (101) MSWD 1.2, probability 0.2

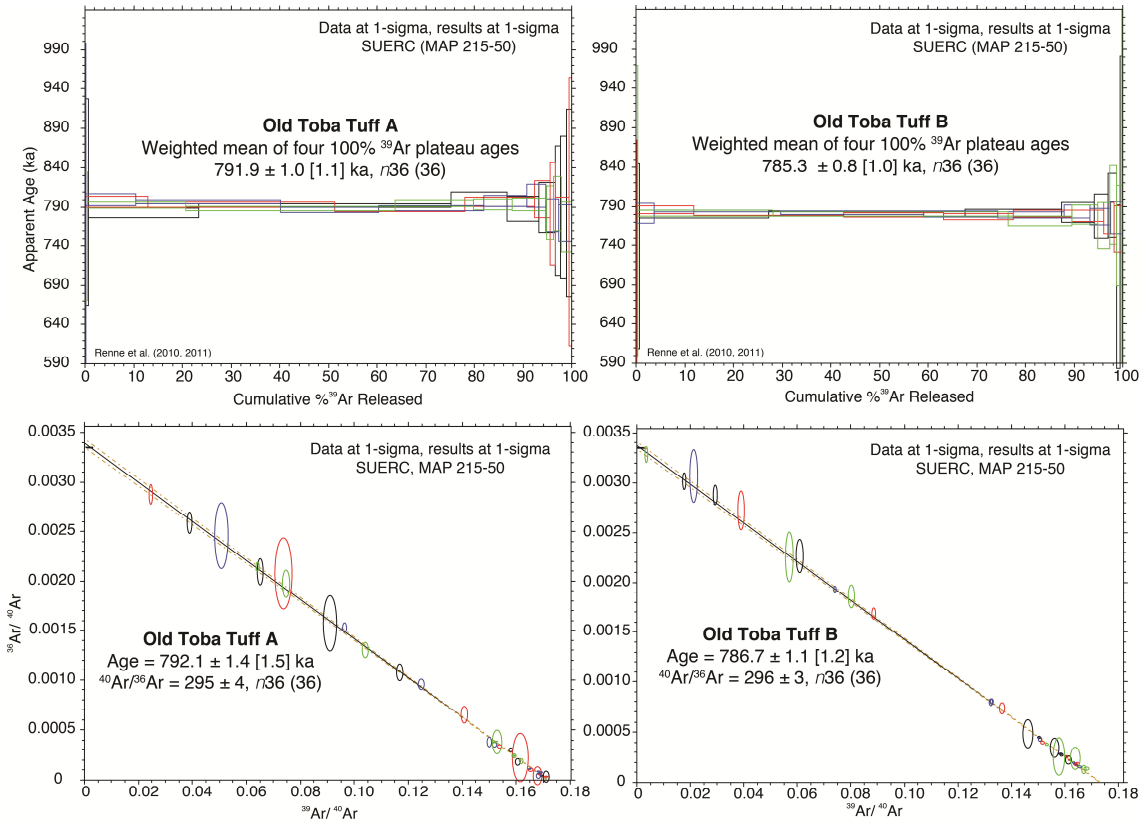

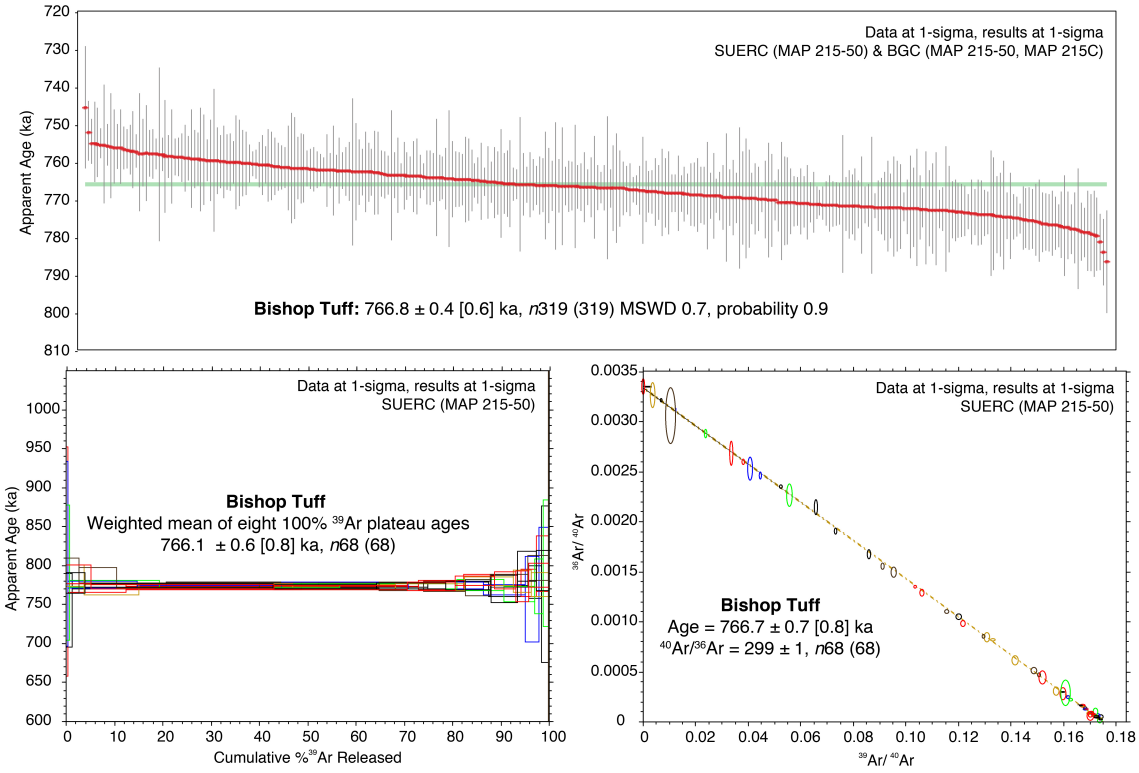

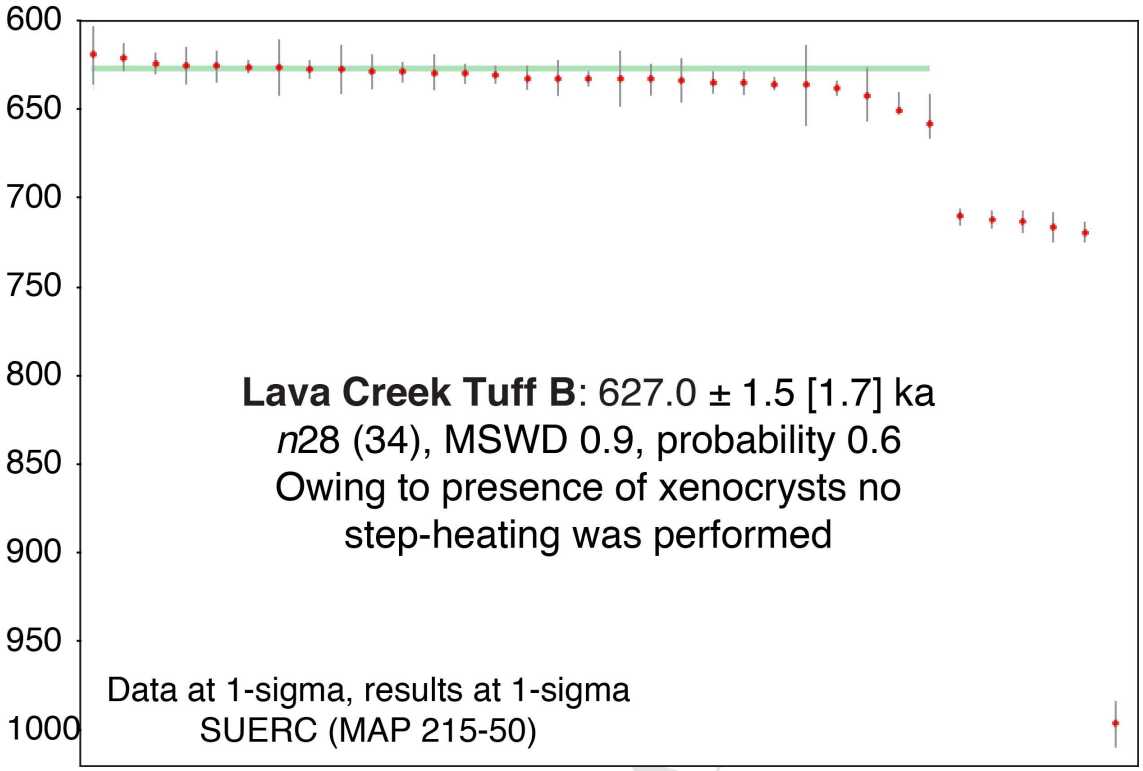

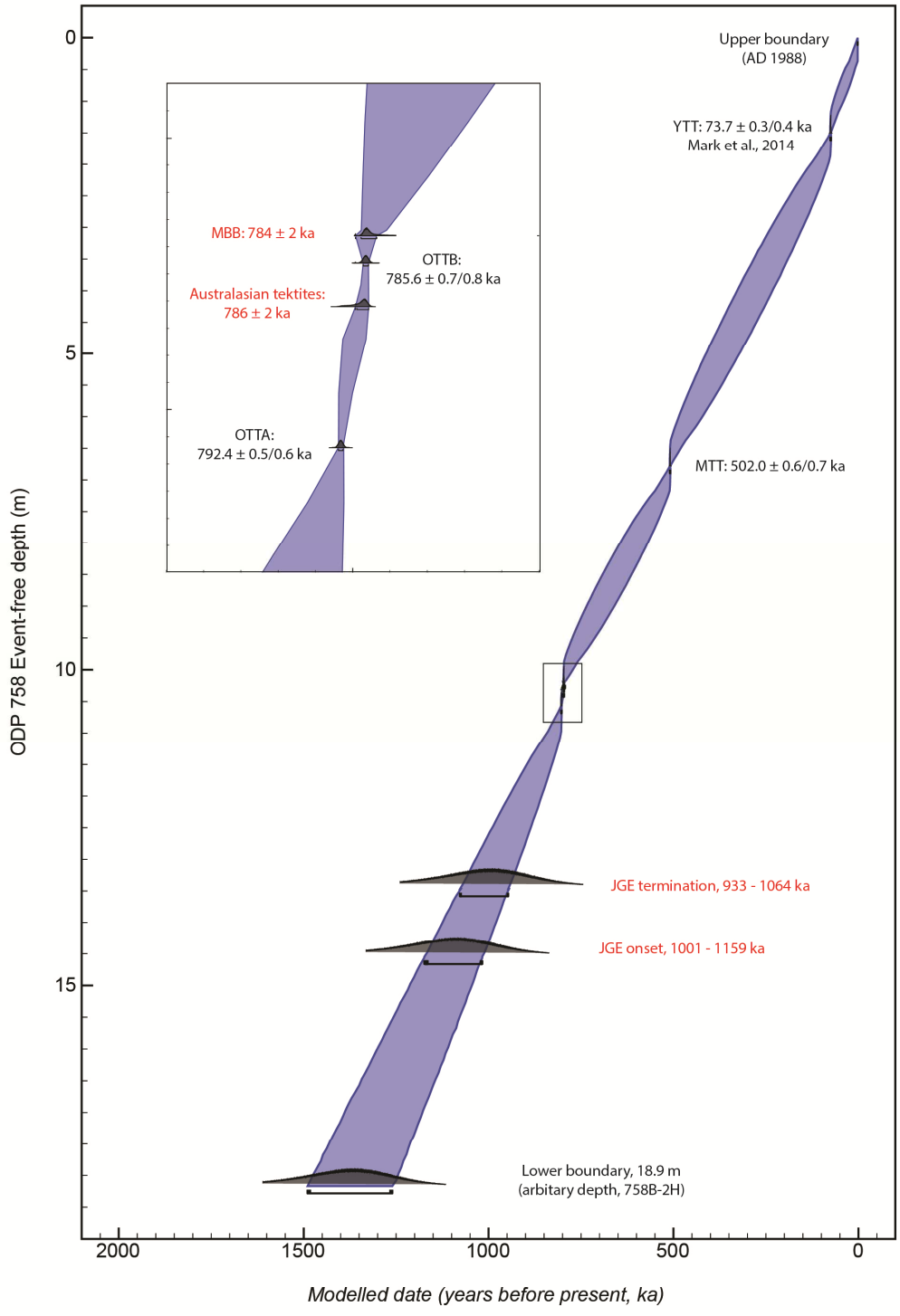
Upper boundary
(AD 1988)
YTT: 73.7 ± 0.3/0.4 ka
Mark et al., 2014
MBB: 784 ± 2 ka
OTTB:
785.6 ± 0.7/0.8 ka
Australasian tektites:
786 ± 2 ka
OTTA:
792.4 ± 0.5/0.6 ka
MTT: 502.0 ± 0.6/0.7 ka
JGE termination, 933 - 1064 ka
JGE onset, 1001 - 1159 ka
Lower boundary, 18.9 m
(arbitary depth, 758B-2H)
ODP 758 Event-free depth (m)
0
5
10
15
2000
1500
1000
500
0
Modelled date (years before present, ka)

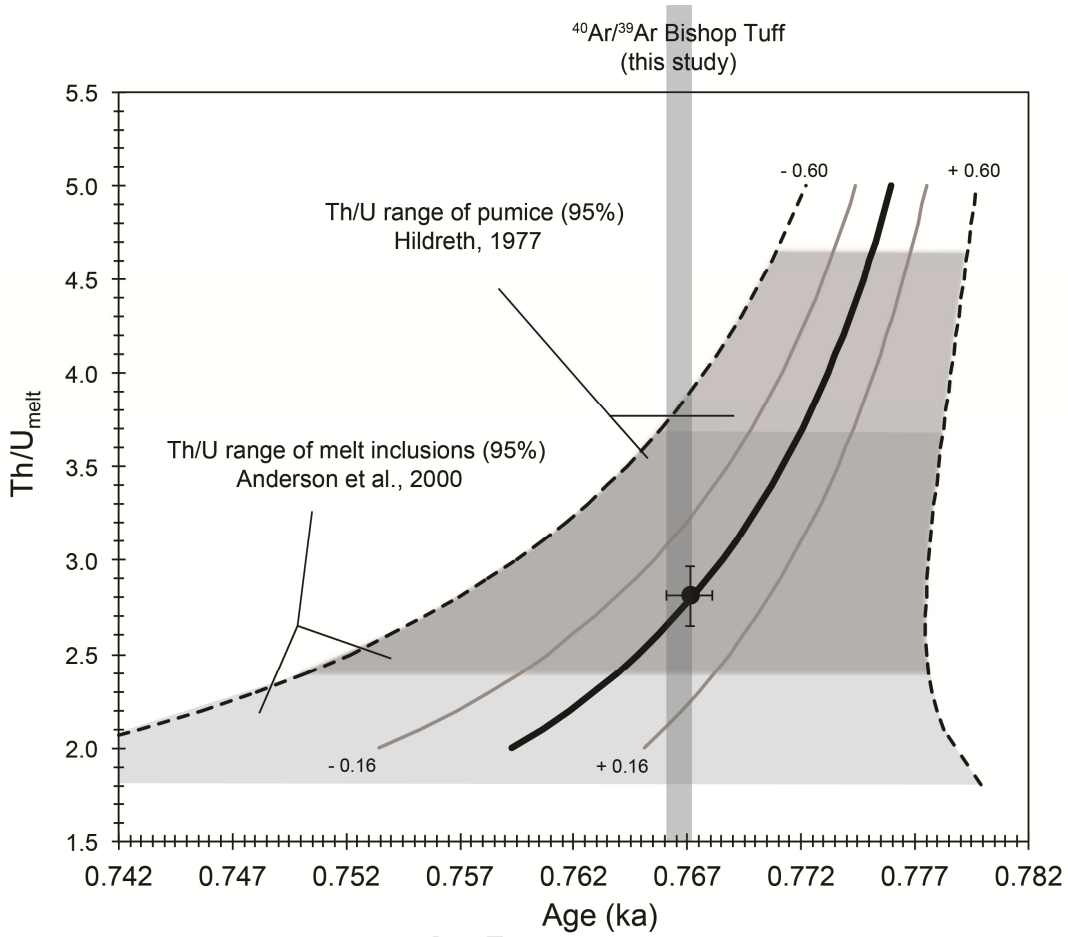
$^{40}Ar/^{39}Ar$ Bishop Tuff
(this study)
Th/U range of pumice (95%)
Hildreth, 1977
Th/U range of melt inclusions (95%)
Anderson et al., 2000
- 0.60
+ 0.60
- 0.16
+ 0.16
Th/U_{melt}
Age (ka)
5.5
5.0
4.5
4.0
3.5
3.0
2.5
2.0
1.5
0.742
0.747
0.752
0.757
0.762
0.767
0.772
0.777
0.782

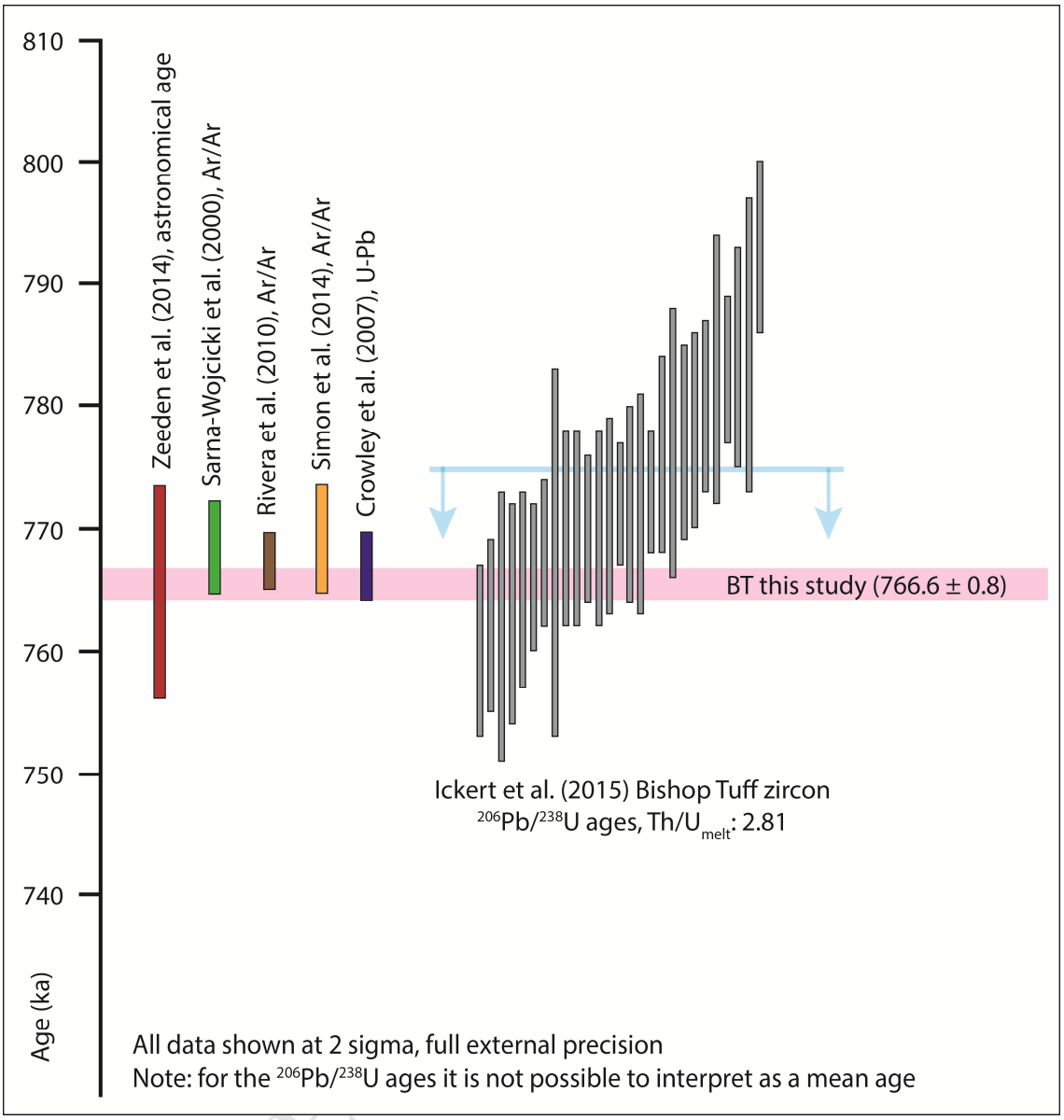
810
800
790
780
770
760
750
740
Age (ka)
Zeeden et al. (2014), astronomical age
Sarna-Wojcicki et al. (2000), Ar/Ar
Rivera et al. (2010), Ar/Ar
Simon et al. (2014), Ar/Ar
Crowley et al. (2007), U-Pb
BT this study (766.6 ± 0.8)
Ickert et al. (2015) Bishop Tuff zircon
$^{206}Pb/^{238}U$ ages, Th/U_{melt}: 2.81
All data shown at 2 sigma, full external precision
Note: for the $^{206}Pb/^{238}U$ ages it is not possible to interpret as a mean age

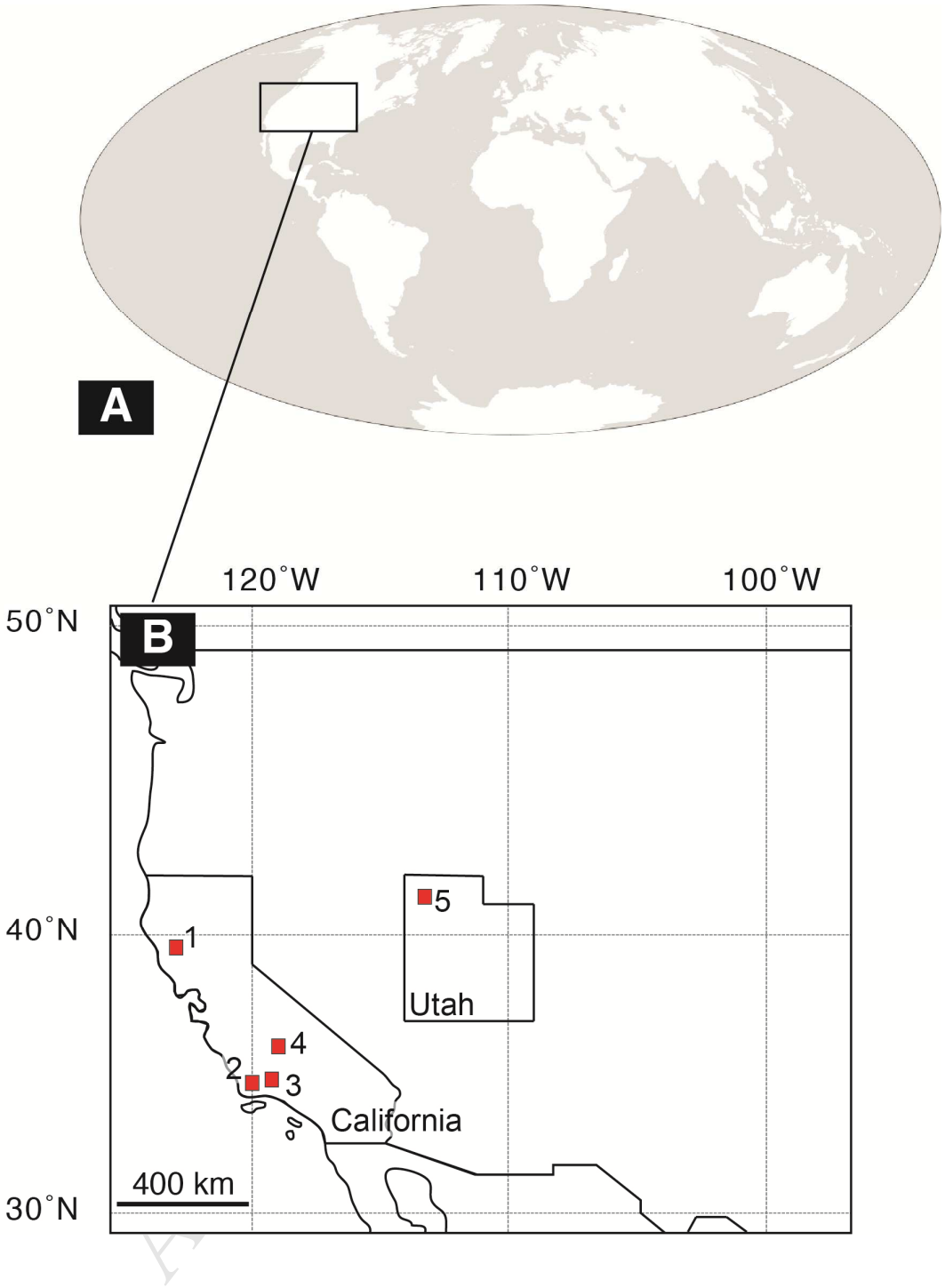
A
B
120˚W
110˚W
100˚W
50˚N
40˚N
30˚N
1
2
3
4
5
Utah
California
400 km

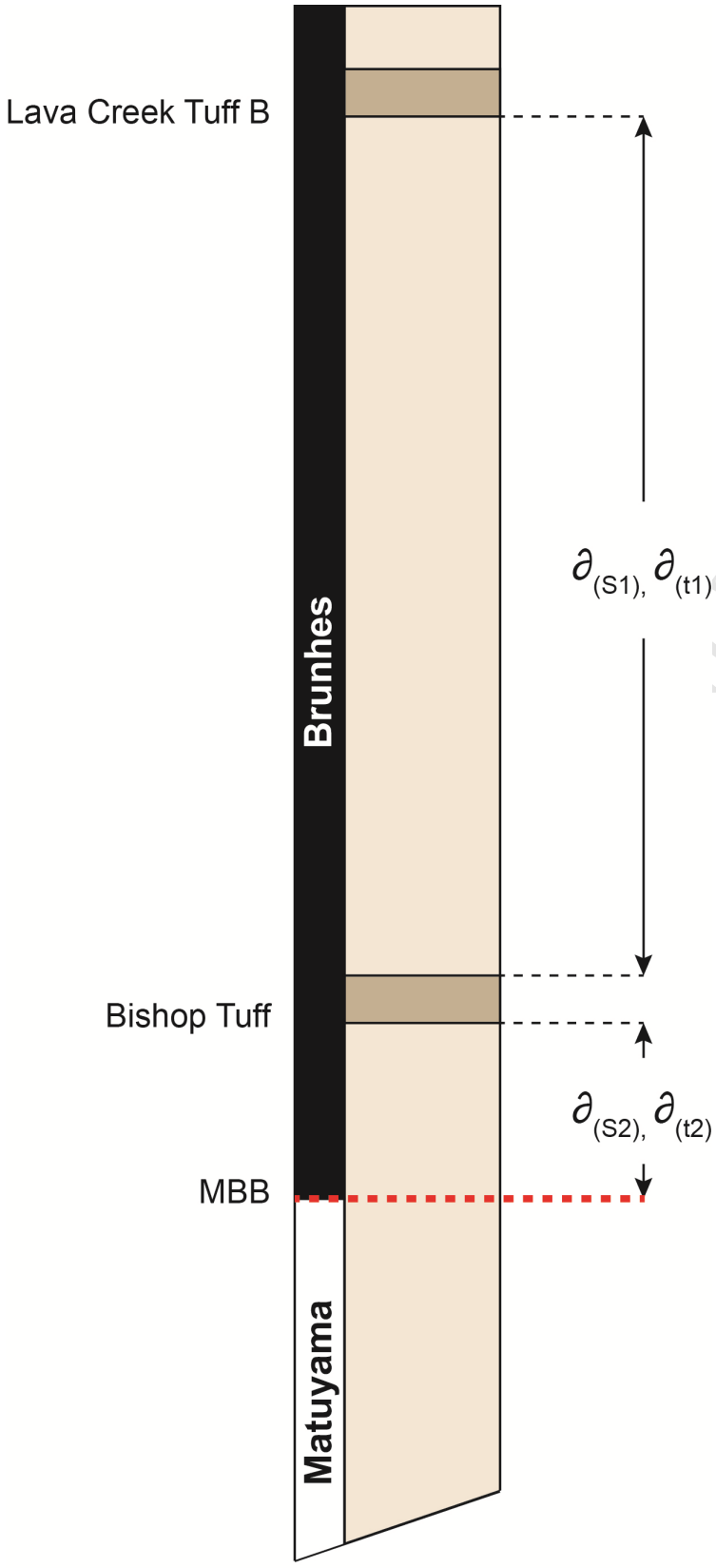
Lava Creek Tuff B
Brunhes
$\partial_{(S1)}, \partial_{(t1)}$
Bishop Tuff
$\partial_{(S2)}, \partial_{(t2)}$
MBB
Matuyama

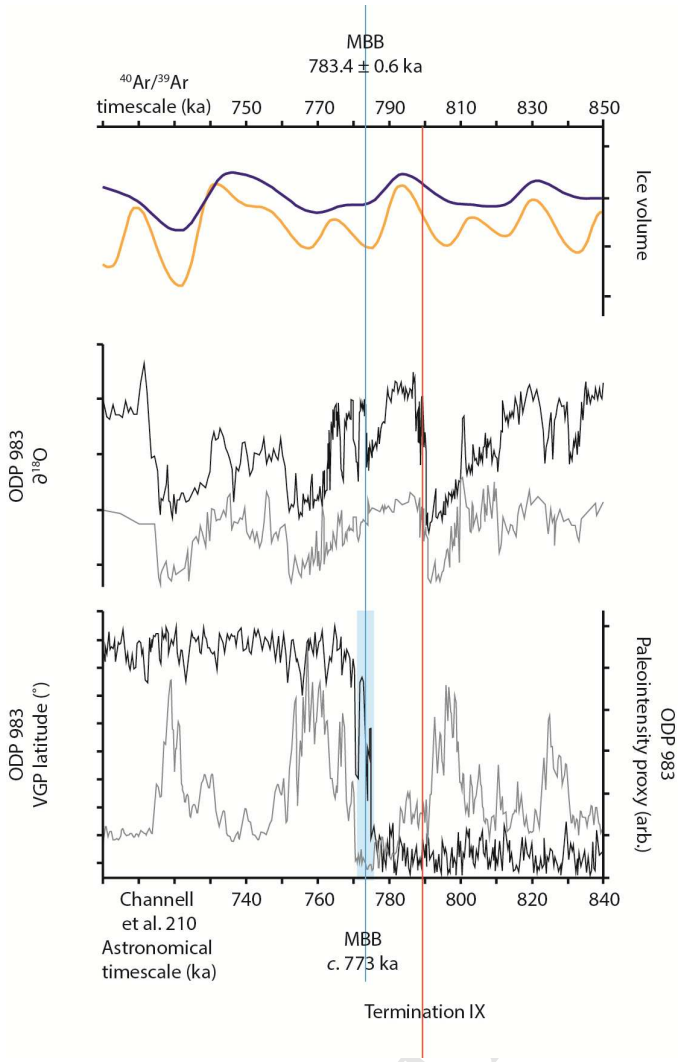

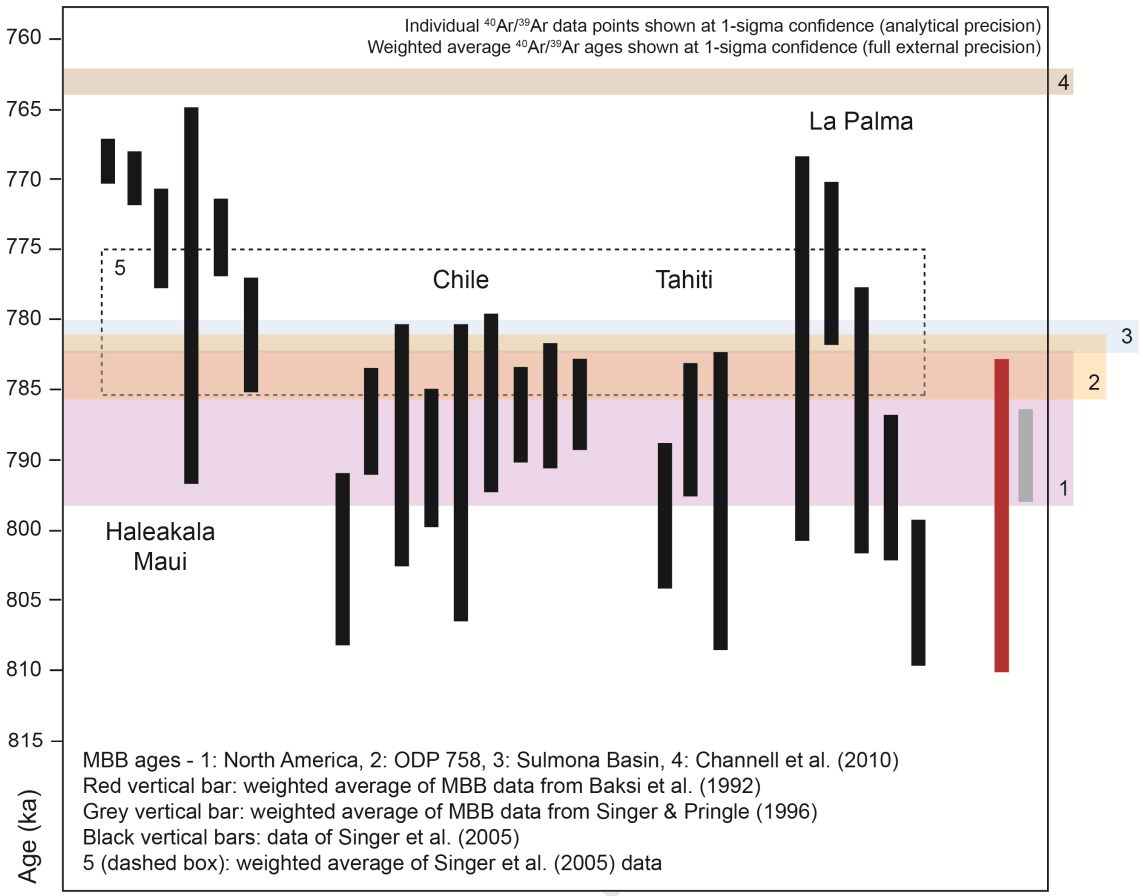

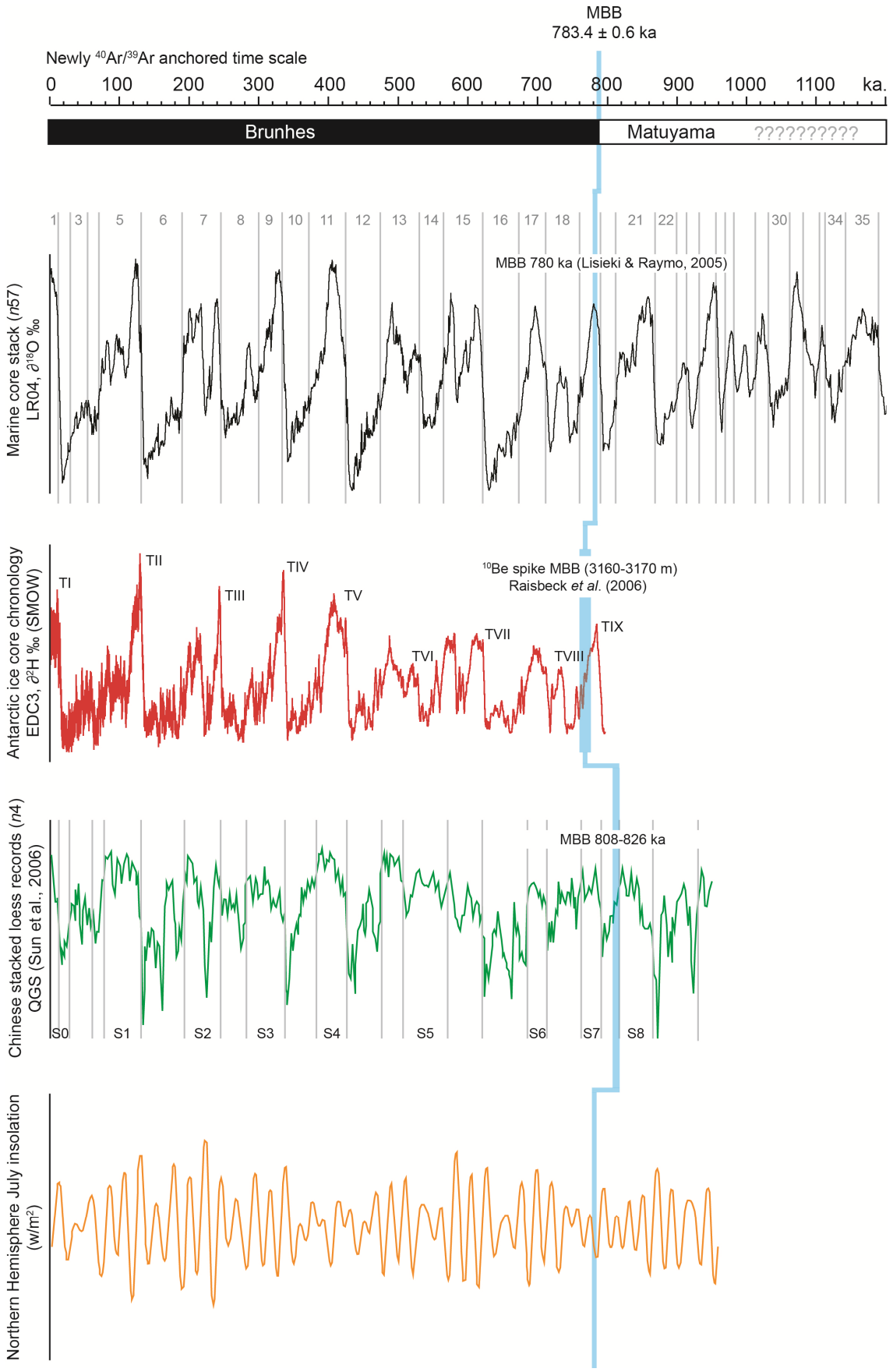
MBB
783.4 ± 0.6 ka
Newly 40Ar/39Ar anchored time scale
0 100 200 300 400 500 600 700 800 900 1000 1100 ka.
Brunhes
Matuyama
??????????
1 3 5 6 7 8 9 10 11 12 13 14 15 16 17 18 21 22 30 34 35
MBB 780 ka (Lisieki & Raymo, 2005)
Marine core stack (n57)
LR04, δ18O ‰
TI
TII
TIII
TIV
TV
TVI
TVII
TVIII
TIX
10Be spike MBB (3160-3170 m)
Raisbeck et al. (2006)
Antarctic ice core chronology
EDC3, δ2H ‰ (SMOW)
MBB 808-826 ka
S0 S1 S2 S3 S4 S5 S6 S7 S8
Chinese stacked loess records (n4)
QGS (Sun et al., 2006)
Northern Hemisphere July insolation
(w/m2)